Available online at www.sciencedirect.com

ScienceDirect

Geochimica et Cosmochimica Acta 135 (2014) 102–125

Geochimica et Cosmochimica Acta

www.elsevier.com/locate/gca

On the $\Delta^{17}O$ budget of atmospheric O_2

Edward D. Young *, Laurence Y. Yeung, Issaku E. Kohl

Department of Earth, Planetary, and Space Sciences, University of California, Los Angeles, Los Angeles, CA, United States

Received 15 September 2013; accepted in revised form 19 March 2014; Available online 31 March 2014

Abstract

We modeled the $\Delta^{17}O$ of atmospheric O_2 using 27 ordinary differential equations comprising a box model composed of the stratosphere, troposphere, geosphere, hydrosphere and biosphere. Results show that 57% of the deficit in ^{17}O in O_2 relative to a reference water fractionation line is the result of kinetic isotope fractionation attending the Dole effect, 33% balances the positive $\Delta^{17}O$ of $O(^1D)$ in the stratosphere, and 10% is from evapotranspiration. The predicted $\Delta'^{17}O$ O_2 relative to waters is $-0.410‰$ as measured at the $\delta^{18}O$ of air. The value for $\Delta'^{17}O$ O_2 varies at fixed $\delta^{18}O$ with the concentration of atmospheric CO_2, gross primary production, and net primary production as well as with reaction rates in the stratosphere. Our model prediction is consistent with our measurements of the oxygen isotopic composition of air O_2 compared with rocks if rocks define a fractionation line with an intercept in $\delta'^{17}O = 10^3\ln(\delta^{17}O/10^3 + 1)$ vs. $\delta'^{18}O = 10^3\ln(\delta^{18}O/10^3 + 1)$ space less than SMOW but more positive than some recent measurements imply. The predicted $\Delta^{17}O$ is less negative than that obtained from recent measurements of O_2 directly against SMOW. Underestimation of $\Delta'^{17}O$ O_2 can only be ameliorated if the integrated (bulk) $\Delta'^{17}O$ for stratospheric CO_2 is significantly greater than measurements currently allow. Our results underscore the need for high-precision comparisons of the $^{17}O/^{16}O$ and $^{18}O/^{16}O$ ratios of atmospheric O_2, VSMOW, and rocks.

1. INTRODUCTION

Molecular oxygen in Earth's atmosphere is not in isotopic equilibrium with the oceans. If it were, it would have $^{18}O/^{16}O$ ratios ~6‰ greater than ocean water (Urey and Grieff, 1935). Rather, $^{18}O/^{16}O$ in atmospheric O_2 is greater than typical ocean water by 23–24‰ (Kroopnick and Craig, 1972; Barkan and Luz, 2005). This excess in heavy isotopes is but one expression of the balance of kinetic processes that controls the abundance and isotopic composition of atmospheric O_2. The elevated $\delta^{18}O$ in O_2 relative to ocean water (here we will use $\delta^{18}O$ is the per mil difference from Standard Mean Ocean Water, SMOW) is referred to as the Dole effect (Dole, 1935) and is the result of a non-equilibrium steady-state between production of O_2 by photosynthesis and preferential uptake of ^{16}O relative to ^{18}O during respiration (Lane and Dole, 1956). Molecular oxygen is also anomalously low in $^{17}O/^{16}O$ relative to waters and rocks (Fig. 1). The paucity of ^{17}O in air O_2 stands out among Earth's oxygen reservoirs. The depletion in ^{17}O was identified by workers using tank-O_2 derived from air as an isotopic standard long before its origin was identified (e.g., Young et al., 1998a,b). We now know that the relatively low $^{17}O/^{16}O$ is primarily the consequence of two factors: (1) a deficit in ^{17}O that offsets the relative excess ^{17}O carried by CO_2 and produced during ozone formation in the stratosphere (Yung et al., 1991; Bender et al., 1994; Luz et al., 1999); and (2) kinetic isotope fractionation associated with respiration (Young et al., 2002). The negative $\Delta^{17}O$ ($\Delta^{17}O$ in general refers to $^{17}O/^{16}O$ relative to a value predicted by the associated $^{18}O/^{16}O$) of atmospheric O_2 is therefore dependent upon a myriad of reaction rates in the stratosphere and troposphere, fluxes between oxygen-bearing reservoirs, and associated isotope fractionation factors. An understanding of the origin of the $\Delta^{17}O$ budget

* Corresponding author. Tel.: +1 310 267 4930.
E-mail address: eyoung@epss.ucla.edu (E.D. Young).

http://dx.doi.org/10.1016/j.gca.2014.03.026
0016-7037/

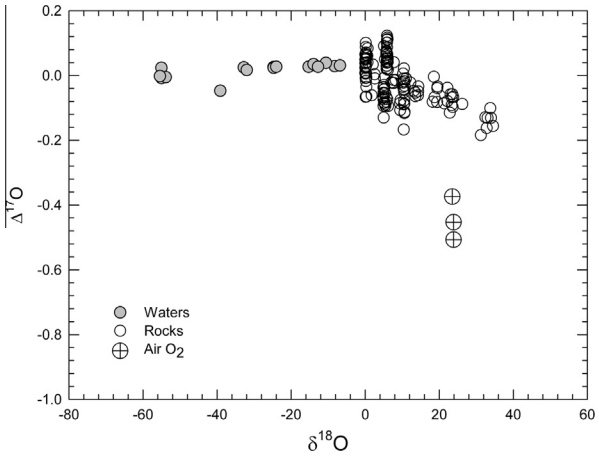

Fig. 1. Plot of $\Delta^{17}O = \Delta'^{17}O = 10^3\ln(\delta^{17}O/10^3 + 1) - 0.528$ $(10^3\ln(\delta^{18}O/10^3 + 1)$ vs. $\delta^{18}O = 10^3\ (([^{18}O/^{16}O)/([^{18}O/^{16}O)_{SMOW} - 1)$ showing the deficit in ^{17}O air O_2 relative to rocks and waters. This deficit is evident regardless of reference frame. This paper addresses the origin of this deficit. The negative slope of the rock data represents a lower fractionation exponent than that for waters (see text). Rock data: Rumble et al. (2007), Tanaka and Nakamura (2012). Water data: Barkan and Luz (2005), Schoenemann et al. (2012), Tanaka and Nakamura (2012). Air data: Barkan and Luz (2005, 2011), this study.

of atmospheric oxygen can come from models that successfully reproduce the measured value. Analogous efforts have been made over the years to reproduce the $^{18}O/^{16}O$ Dole effect (e.g., Bender et al., 1994; Hoffman et al., 2004).

Calculations to assess the magnitude of molecular oxygen $\Delta^{17}O$ have been made previously (e.g., Luz et al., 1999; Blunier et al., 2002; Cao and Bao, 2013). However, there are no existing models, to our knowledge, that consider a large range of the relevant factors in both the stratosphere and troposphere. Blunier et al., for example, concentrate on tropospheric/land/ocean effects. Cao and Bao (2013) focus on the long timescales and unusually large $\Delta^{17}O$ effects, allowing for approximations not applicable to studies in the present-day. The controls on $\Delta^{17}O$ of atmospheric O_2 include: (1) the $^{17}O/^{16}O$ and $^{18}O/^{16}O$ isotope fractionation associated with respiration; (2) isotope fractionations associated with leaf water; (3) the rate of photosynthesis (gross primary productivity); (4) the rate of respiration; (5) the rates of ozone formation and destruction in the stratosphere; (6) the rate of formation and quenching of excited-state atomic oxygen, $O(^1D)$, in the stratosphere; (7) CO_2 concentrations driven by short and long-term carbon budgets; (8) the rate at which oxygen isotopes are transferred from $O(^1D)$ to CO_2 in the stratosphere; (9) mixing rates between stratosphere and troposphere; and (10) the rate of CO_2–H_2O oxygen isotope exchange at ground level.

In this study we construct a model from the essential rates affecting $\Delta^{17}O$ of atmospheric O_2. Our goal is to compare this model to measurements of the $\Delta^{17}O$ of O_2 in air relative to a suitable reference. Over the past decade, use of $\Delta^{17}O$ in O_2 as a proxy for gross primary production (GPP), as suggested by Luz et al. (1999), has given rise to the practice of using atmospheric O_2 itself as the oxygen isotope standard. Of course the isotopic composition of air O_2 today is composed of one datum and so cannot be used *a priori* to define a fractionation line in three-isotope space. The range of values in oxygen three-isotope space (i.e., $\delta^{17}O$ vs. $\delta^{18}O$) due to different processes must be inferred and will have been different if, for example, the ratios of different respiration pathways varied in the past. In this work our goal is to gauge the magnitude of the ^{17}O deficit in air relative to a standard material that has fixed oxygen isotopic ratios by virtue of being immune to the factors that alter the isotopic composition of O_2. Earth's waters (ocean water, precipitation) could serve as such a standard. We will make use of the water reference because it has been used by many authors and because its oxygen three-isotope mass fractionation characteristics are well documented (Meijer and Li, 1998; Barkan and Luz, 2005; Tanaka and Nakamura, 2012).

Waters, however, are not precisely representative of the bulk Earth in $\Delta^{17}O$ (Tanaka and Nakamura, 2012; Pack and Herwartz, 2014) and in principle can vary with processes like diffusion (although such variations are small) (Luz and Barkan, 2010). In addition, measuring the triple oxygen isotopic composition of waters is not routine (comparatively few laboratories actually measure the $^{18}O/^{16}O$ and $^{17}O/^{16}O$ of their intralaboratory reference gas relative to O_2 generated from VSMOW). Rocks, on the other hand, are measured in many laboratories, and there is a wealth of triple oxygen isotope data for rocks with compositions comparable to the high $\delta^{18}O$ values of O_2 in air (Fig. 1) that define well-characterized fractionation lines (Miller, 2002; Pack et al., 2007; Rumble et al., 2007). Rocks can therefore provide a stable "measuring stick" against which to gauge the isotopic composition of air while minimizing extrapolations and eliminating the need to infer three-isotope effects.

In this study we report measurements of $\delta^{17}O$ and $\delta^{18}O$ values for atmospheric O_2 and rocks obtained over several years as a test of our understanding of the O_2 $\Delta^{17}O$ budget. The absence of such comparisons in the literature has made it difficult to assess whether or not the $\Delta^{17}O$ budget for O_2 can truly be balanced.

Comparing the oxygen isotopic compositions of rocks and air has been criticized in the past as being irrelevant to the composition of air owing to the lack of air-rock oxygen exchange (Angert et al., 2003). The value of comparing air to rock is not that these reservoirs exchange oxygen, but precisely that they do not (on 10^3 to 10^4 year timescales and less); the ideal measuring stick is not affected by the object to be measured. In the long-term, however, the notion that air and rocks are decoupled is invalid. The ultimate source of O_2 in air is ocean water and meteoric waters derived from the oceans. The oxygen isotopic composition of ocean water is controlled by a balance between high and low-temperature water–rock reactions in the ocean basins on timescales of hundreds of millions of years (Muehlenbachs and Clayton, 1976). Therefore, departures in water and air $\Delta^{17}O$ values from those defined by equilibrium with rocks (ocean basalts in particular) trace the other processes by which these reservoirs evolve operating on much shorter

timescales. We view rocks as a useful measuring stick in this context. We are interested only in the difference between $\Delta^{17}O$ of atmospheric O_2 and rock for the purposes of balancing the oxygen isotope budget of the atmosphere. Rocks are not useful as a practical reference when trying to measure small changes in molecular oxygen $\Delta^{17}O$ where shifts in $\delta^{18}O$ alone cause apparent shifts in $\Delta^{17}O$ relative to rock (due to different fractionation slopes, Section 2). We do not advocate using rock as a reference for estimating GPP from $\Delta^{17}O$ in O_2 dissolved in ocean waters, for example.

The paper is organized as follows: In Section 2 we examine the details of mass fractionation laws and reservoir effects relevant to respiration and the isotopic composition of O_2. We present the model for $\Delta^{17}O$ of atmospheric O_2 and evaluate the inputs to the model in Section 3. Section 4 is a summary of the model results and discussion of the implications. We compare the predictions of the model with our measurements of air and rock oxygen isotope ratios in Section 5. In Section 6 we consider the leeway for adjustments to the model inputs in view of measurements and we present our conclusions in Section 7.

2. FRACTIONATION LAWS AND RESERVOIR EFFECTS

2.1. Mass fractionation laws

The major component of the deviation in $\Delta^{17}O$ of atmospheric O_2 from waters and rocks is the mass-dependent fractionation law associated with respiration. For a proper evaluation of this effect we must understand the basic relationships that comprise mass-fractionation laws in three-isotope space.

Mass-dependent isotope fractionation involving three isotopes is characterized by an exponent relating the two fractionation factors. In the case of oxygen the two fractionation factors are

$$\frac{(^{18}O/^{16}O)}{(^{18}O/^{16}O)_0} = \frac{^{18}R}{^{18}R_0} = \alpha_{18} \quad (1)$$

and

$$\frac{(^{17}O/^{16}O)}{(^{17}O/^{16}O)_0} = \frac{^{17}R}{^{17}R_0} = \alpha_{17} \quad (2)$$

where the subscript 0 refers to an initial condition or some other reference state (including another phase). The two fractionation factors α are related by the following mass fractionation "law":

$$\alpha_{17} = (\alpha_{18})^{\beta}. \quad (3)$$

We have used the exponent designation β following Young et al. (2002) (alternative terminologies are discussed below). Hulston and Thode (1965) recognized that the linear relationship between $\ln(\alpha_{17})$ and $\ln(\alpha_{18})$ in Eq. (3) can be preserved using a modification of the commonly used delta notation. The usual definition of the parameter describing a per mil fractional difference in isotope ratio is $\delta^i = 10^3 ({}^iR/{}^iR_o - 1)$ for rare isotope i. It is convenient to replace this definition with a logarithmic variant: $\delta'^i = 10^3 \ln({}^iR/{}^iR_o)$. In the case of oxygen the latter "delta-prime" has been referred to variously in the literature as $\ln(\delta^i + 1)$ where the factor of 10^3 is implicitly omitted (e.g., Luz and Barkan, 2005), or $\ln{}^iO$ (e.g., Wiegel et al., 2013). Note that $\delta'^i = 10^3 \ln(\alpha_i)$ so the mass fractionation law in Eq. (3) can be written as

$$\delta'^{17}O = \beta\, \delta'^{18}O - (\delta'^{17}O_{ref} + \beta\, \delta'^{18}O_{ref}) \quad (4)$$

where the reference composition (ref) is any point on the fractionation line defined by Eq. (4). The linear relationship between logarithmic delta values in Eq. (4) is convenient for describing mass fractionation behavior in oxygen three-isotope space. It also makes the definition of $\Delta^{17}O$ simple:

$$\Delta'^{17}O = \delta'^{17}O - \beta\, \delta'^{18}O + (\delta'^{17}O_{ref} + \beta\, \delta'^{18}O_{ref}). \quad (5)$$

For many applications the last term (the intercept in parentheses) vanishes as the reference value can be taken to be the origin. For precision of presentation we will use the prime symbol to denote $\Delta^{17}O$ values calculated from Eq. (5).

Values for the exponent β vary depending upon the process. Where the fractionation factors refer to equilibrium partitioning of oxygen isotopes $\beta \sim (1/m_{16} - 1/m_{17})/(1/m_{16} - 1/m_{18})$ where m_i is the atomic mass of isotope i (Young et al., 2002). A comprehensive method for calculating β for equilibrium fractionation, including temperature dependencies, is given by Cao and Liu (2011). For non-equilibrium processes the values for β are usually lower than the equilibrium values and given by the expression $\beta = \ln(M_{16}/M_{17})/\ln(M_{16}/M_{18})$ where M_i are the reduced masses, molecular masses, or any mass in motion for the kinetic process at hand (Young et al., 2002).

In what follows we will use the term "intrinsic" to refer to fractionation resulting from a process of interest. This process of interest (e.g., respiration) may in fact be composed of numerous elementary steps (diffusion, bond rupture, and so forth) with each step having its own associated fractionation (e.g., Hayes, 2001), but our concern here is the observable fractionation for the net process. We will use the term "effective" to refer to observed fractionations resulting from the process of interest convolved with the effects imposed by mechanisms of mass transfer. The latter are referred to as "reservoir effects." Values for β intrinsic to the isotope fractionation process itself do not always describe the slope in $\delta^{17}O'$ vs. $\delta^{18}O'$ space because of reservoir, or mass-balance, effects, as described below.

2.2. Closed-system steady-state reservoir effects

The presence or absence of reservoir effects on the effective value of β in Eq. (4) is particularly important for assessing the magnitude of $\Delta'^{17}O$ in air. As an illustration we consider a very simple two-box model for the production of O_2 from water by photosynthesis and consumption of O_2 by respiration in a closed system. The two rate equations comprising this closed-system model are

$$\begin{aligned}\frac{dn^{\rm air}_{\rm O_2}}{dt} &= k_p n_{\rm H_2O} - k_r n^{\rm air}_{\rm O_2}\\ \frac{dn_{\rm H_2O}}{dt} &= -k_p n_{\rm H_2O} + k_r n^{\rm air}_{\rm O_2}\end{aligned} \tag{6}$$

where k_r is the respiration rate constant and k_p is the photosynthesis rate constant. The solution for time-dependent evolution of air O_2 is

$$n(t)^{\rm air}_{\rm O_2} = \left(\frac{k_r}{k_r+k_p} n^{0,\rm air}_{\rm O_2} - \frac{k_p}{k_p+k_r} n^{0}_{\rm H_2O}\right) e^{-(k_r+k_p)t} + \frac{k_p}{k_p+k_r}(n^{0,\rm air}_{\rm O_2} + n^{0}_{\rm H_2O}) \tag{7}$$

where the superscript 0 signifies the initial condition. The steady-state solution is then

$$\lim_{t\to\infty} n(t)^{\rm air}_{\rm O_2} = \frac{k_p}{k_p+k_r}(n^{0,\rm air}_{\rm O_2} + n^{0}_{\rm H_2O}). \tag{8}$$

Because respiration produces a significant kinetic isotope effect, α_{18}, the analogous expression for $n^{\rm air}_{^{18}O^{16}O}$ (where $^{18}O^{16}O/^{16}O_2$ represents $(^{18}O^{16}O + {}^{16}O^{18}O)/^{16}O_2$ and $^{34}R = 2^{18}R$ to a good approximation) is obtained by replacing k_r with $\alpha_{18}k_r$. The ratio $^{18}O^{16}O/^{16}O_2$ at steady state is therefore

$$\frac{n^{\rm air}_{^{18}O^{16}O}}{n^{\rm air}_{^{16}O_2}} = \frac{\left(\frac{k_p}{k_p+\alpha_{18}k_r}\right)}{\left(\frac{k_p}{k_p+k_r}\right)} 2^{18}R_0 = \frac{\left(1+\frac{k_r}{k_p}\right)}{\left(1+\alpha_{18}\frac{k_r}{k_p}\right)} 2^{18}R_0 \tag{9}$$

where $^{18}R_0$ is the initial isotope ratio for all species. Similarly for $^{17}O^{16}O$

$$\frac{n^{\rm air}_{^{17}O^{16}O}}{n^{\rm air}_{^{16}O_2}} = \frac{\left(\frac{k_p}{k_p+\alpha^{\beta}_{18}k_r}\right)}{\left(\frac{k_p}{k_p+k_r}\right)} 2^{17}R_0 = \frac{\left(1+\frac{k_r}{k_p}\right)}{\left(1+\alpha^{\beta}_{18}\frac{k_r}{k_p}\right)} 2^{17}R_0. \tag{10}$$

In the case of $^{18}O^{16}O/^{16}O_2$ fractionation the effective fractionation factor that would be observed by sampling O_2 is

$$\alpha_{18,\rm eff} = \frac{\left(1+\frac{k_r}{k_p}\right)}{\left(1+\alpha_{18}\frac{k_r}{k_p}\right)}. \tag{11}$$

This is an example of a reservoir effect on a fractionation factor. If we consider the simplest possible kinetic model such that $\alpha_{18} = \sqrt{m_{16_O}/m_{18_O}} = 0.9426$ (i.e., −57‰) and $k_r/k_p = ½$ (a typical ratio), $\alpha_{18,\rm eff} = 1.0195$. In other words, the effective fractionation due to respiration operating with photosynthesis in a closed system would be 19.5‰ if the fractionation attributable to respiration alone is −57‰. We present this for illustration only with no implication that the respiration/photosynthesis reaction couple behaves as a closed system in nature (it does not).

More importantly for the subject of this paper, the $\Delta'^{17}O$ of atmospheric O_2, the β relating the three isotopologues of O_2 in this example is also changed and is

$$\beta_{\rm eff} = \frac{\delta'^{17}O}{\delta'^{18}O} = \frac{\ln\left(\frac{1+k_r/k_p}{1+\alpha^{\beta}_{18}k_r/k_p}\right)}{\ln\left(\frac{1+k_r/k_p}{1+\alpha_{18}k_r/k_p}\right)}. \tag{12}$$

The slope in Eq. (4) relating $\delta'^{17}O$ to $\delta'^{18}O$ is now $\beta_{\rm eff}$. Returning to our simple model where fractionation is based on atomic masses, the β for respiration alone would be $\ln(m_{16}/m_{17})/\ln(m_{16}/m_{18}) = 0.516$, but for the same α_{18} and k_r/k_p above, $\beta_{\rm eff} = 0.521$. This difference of 0.005 in β causes a shift in $\Delta'^{17}O$ of $10^3\ln(1.0195)$ (0.521–0.516) = 0.097‰, a significant number.

2.3. Rayleigh fractionation reservoir effects

The closed-system steady-state example above illustrates just one form of a reservoir effect. In that case the modifications to the fractionation factors arise from a dilution of the intrinsic fractionation in one direction by the lack of fractionation in the other and the reciprocity induced by the exchange of isotopes between the reservoirs. A similar but different change in effective fractionation occurs for Rayleigh fractionation. This is understood to be again the consequence of changes in two complimentary reservoirs as reaction proceeds, in this case the residue (res) and fractionate (frac). In order to see this consider that the starting point for the derivation of the Rayleigh equation is $dn_{i,\rm res} + dn_{i,\rm frac} = 0$ for all isotope species i (Young, 2001). If this reciprocity does not apply, the fractionation is not a Rayleigh process.

We consider removal of O_2 from air by respiration alone by Rayleigh fractionation. This case has been invoked to extract fractionation laws for respiration from experimental data (Angert et al., 2003). In this case we have

$$\frac{^{18}R}{^{18}R_0} = F^{\alpha_{18}-1} \tag{13}$$

and

$$\frac{^{17}R}{^{17}R_0} = F^{(\alpha_{18})^{\beta}-1} \tag{14}$$

where F is the fraction of O_2 remaining in air (actually the fraction of $^{32}O_2$). The resulting fractionation law is, using simple properties of logarithms of exponents

$$\beta_{\rm eff} = \frac{\delta'^{17}O}{\delta'^{18}O} = \frac{\ln(^{17}R/^{17}R_0)}{\ln(^{18}R/^{18}R_0)} = \frac{\alpha^{\beta}_{18}-1}{\alpha_{18}-1}. \tag{15}$$

Here the result is similar to the 2-box model; the effective exponent is greater than the pure single-process β. Using again our fictive respiration α of 0.9426 and $\beta = 0.516$, the $\beta_{\rm eff}$ is 0.526 (cf. our 2-box model result where $\beta_{\rm eff} = 0.521$). In both of these cases, $\beta_{\rm eff}$ is substantially greater than the intrinsic β although the two effective values are not identical. Within the context of our simple example, we can envision an experiment in which O_2 is removed by respiration and then replaced by photosynthesis and respiration in concert in a closed system, achieving a steady-state mixing ratio and $\delta'^{18}O$ value similar to the initial condition (e.g., Luz et al., 1999). The result would be a measurable shift in $\Delta'^{17}O$ with no shift in $\delta'^{18}O$. The shift in our example is calculable from the effective fractionation factor for $^{18}O/^{16}O$ and the difference in effective exponents and is $10^3\ln(1.0195)$ (0.526–0.521) =

0.097‰. Such a shift due solely to a change in β_{eff} has been referred to as a "chess move" in three-isotope space (Thiemens, pers. comm.). Similar examples were described by Young et al. (2002).

2.4. Absence of reservoir effects

Intrinsic β values, rather than β_{eff} values, will define slopes on plots of $\delta'^{17}O$ vs. $\delta'^{18}O$ when reservoir effects are eliminated. Removal of reservoir effects occurs when one of the reservoirs becomes impervious to changes in composition. A reservoir that is composed of orders of magnitude more of the isotopes of interest than the others will exhibit this behavior. Modifying our example represented by Eq. (6), we can consider the case of removal of O_2 by respiration with continual replacement by photosynthesis but with a water reservoir (the source of photosynthetic oxygen) that itself is continually replaced by virtue of its great abundance. The isotopic composition of water is therefore unaffected by this process (e.g., $^{18}O/^{16}O$ of the oceans is unaffected by photosynthesis). Because $dn_{H_2O} \sim 0$ not because of a steady state but because of sheer mass, and the rate of photosynthesis is now constant such that $k_p n_{H_2O} = r_p$, our two equations reduce to a single equation:

$$\frac{dn^{air}_{O_2}}{dt} = -k_r n^{air}_{O_2} + r_p \tag{16}$$

where r_p is the fixed rate of photosynthesis for the $^{16}O_2$-isotopologue. At steady state we have

$$k_r n^{air}_{O_2} = r_p \tag{17}$$

and

$$n^{air}_{O_2} = \frac{r_p}{k_r}. \tag{18}$$

The analogous expressions for the two singly-substituted isotopologues are

$$\begin{aligned} n^{air}_{^{18}O^{16}O} &= \frac{r_p 2^{18}R_0}{\alpha_{18} k_r} \\ n^{air}_{^{17}O^{16}O} &= \frac{r_p 2^{17}R_0}{(\alpha_{18})^{\beta} k_r} \end{aligned} \tag{19}$$

and the isotopologue ratios are

$$\begin{aligned} \frac{n^{air}_{^{18}O^{16}O}}{n^{air}_{^{16}O_2}} &= \frac{2^{18}R_0}{\alpha_{18}} \\ \frac{n^{air}_{^{17}O^{16}O}}{n^{air}_{^{16}O_2}} &= \frac{2^{17}R_0}{(\alpha_{18})^{\beta}} \end{aligned}. \tag{20}$$

Since Eq. (20) are the usual relationships between molecular isotopologue ratios and isotope atomic ratios, we see that in this case of an effectively infinite reservoir exchanging with O_2, the fractionation factors are unchanged ($\alpha_{eff} = \alpha$). Because $^{18}R/^{18}R_0 = 1/(\alpha_{18})$ and $^{17}R/^{17}R_0 = 1/(\alpha_{18})^{\beta}$, it follows that

$$\frac{\delta'^{17}O}{\delta'^{18}O} = \frac{\ln(^{17}R/^{17}R_0)}{\ln(^{18}R/^{18}R_0)} = \frac{\beta \ln(1/\alpha_{18})}{\ln(1/\alpha_{18})} = \beta \tag{21}$$

and so $\beta_{eff} = \beta$. A similar analysis involving uptake of O_2 by respiration alone, but with no Rayleigh effect (i.e., uptake by an $\sim$ infinite reservoir), also yields $\alpha_{eff} = \alpha$ and $\beta_{eff} = \beta$. Whenever the reciprocity of reservoirs exchanging with one another is removed, intrinsic fractionation laws are expressed in observed shifts in isotope ratios.

2.5. Terminology

In the present case we need to determine the fractionation law that applies to respiration in nature from fractionations observed in the laboratory because the latter can be measured while the former cannot. It is clearly important to know the role that reservoir effects play in the laboratory and in natural systems if one is to use laboratory experiments to infer fractionation laws for natural systems. However, it is not always possible to determine whether β or a β_{eff} is controlling the relationship between $\delta'^{17}O$ and $\delta'^{18}O$ in a data set. For this reason it has been common practice to replace β in Eq. (4) with the more generic symbol λ (Meijer and Li, 1998; Miller, 2002) without specifying whether λ represents β or β_{eff}. In addition, a number of other symbols have been invoked in the literature to describe different origins for slopes relating $\delta'^{17}O$ and $\delta'^{18}O$. An explanation of the various symbols and their usage is provided by Angert et al. (2003). Arguably, not all of these symbols are required and the "alphabet soup" of letters can be confusing for all but the dedicated practitioners.

What is worse, the various symbols can also result in ambiguity. For example, Angert et al. appear to define θ as the intrinsic exponent β. However, confusion arises because these authors assert that $\lambda = \theta$ at "steady state." From the preceding discussion it is clear that $\lambda \neq \beta$ in the steady state example, and that instead $\lambda = \beta_{eff}$ (e.g., Eq. (12)). Therefore, $\lambda \neq \theta$ at steady state if $\theta = \beta$. Rather, again using the terminology employed by Angert et al., $\lambda = \theta$ when the reciprocity of the reservoirs is eliminated. The problem is circumvented if, in general, $\theta = \beta_{eff}$ and not necessarily β, but then there is no distinction between β and β_{eff} and the role of reservoir effects becomes obscured. The distinction between "steady-state" slopes and "kinetic slopes" has persisted in subsequent work (e.g., Luz and Barkan, 2005) and the meaning of this distinction in terms of β and β_{eff} warrants clarification in future work.

Angert et al. also derive the equivalent of Eq. (15) for Rayleigh fractionation and assign this particular form of β_{eff} the symbol γ after Blunier et al. (2002). They conclude that $\lambda = \gamma$ when the process is one of O_2 consumption alone. To the extent that uptake alone is a Rayleigh process, this equivalency obtains. Angert et al. indicate that their dark respiration experiments in which O_2 is consumed by respiration are Rayleigh in nature (with the implicit assumption being that $dn_{^{18}O,residual} + dn_{^{18}O,fractionate} = 0$, for example). They therefore correct their observed slopes relating $\delta'^{17}O$ and $\delta'^{18}O$ in their dark respiration experiments by solving Eq. (15) for β:

$$\beta = \frac{\ln(\beta_{eff}\alpha_{18} - \beta_{eff} + 1)}{\ln(\alpha_{18})} \tag{22}$$

or, using their symbols

$$\theta = \frac{\ln(\gamma\alpha_{18} - \gamma + 1)}{\ln(\alpha_{18})}. \quad (23)$$

To the extent that the O_2 uptake in these experiments is a Rayleigh process, the θ values reported by Angert et al. are β values for dark respiration, and we take them to be exponents free from reservoir effects.

2.6. Application to respiration on a global scale

Because Earth's reservoirs of water taken as a whole contain far more oxygen than does the atmosphere, we conclude that the correct fractionation law for global respiration is one based on the intrinsic β for respiration and not a form of β_{eff}. This is the correct fractionation law to the extent that the assumption that Earth's oceans and meteoric waters are not affected by the uptake of oxygen by respiration is valid. This is a safe assumption because even if the isotopic composition of a small amount of water is altered by isotope exchange, that water is rapidly replaced (e.g., by rainfall or ingress of soil water). The θ values reported by Angert et al. (2003) and revised by Helman et al. (2005) are taken to be the required β values.

Angert et al. (2003) report β (their θ) values of 0.516, 0.514 and 0.506 for the cytochrome pathway (COX), alternative pathway (AOX), and photorespiration (PR), respectively. Helman et al. (2005) revised the value for photorespiration to 0.512. Using the global fractions of respiration pathways used by Angert et al. (COX = 68%, AOX = 8%, PR = 24%) we calculate a global mean β value for respiration of 0.5149. Different relative fractions of these pathways alter the β value. Using the values in Table 1 of Blunier et al. (2002), for example, results in a value of 0.5143, suggesting that there is uncertainty on the order of *at least* ~0.0005 in the global respiration β even if the measured values for each respiration pathway are known perfectly.

Table 1
Species tracked in the numerical box model. The 27 ordinary differential equations dn_i/dt for each species comprise the model where n_i is the moles of species i. Brackets signify total atoms in unspecified form.

O	Stratosphere
^{17}O	Stratosphere
^{18}O	Stratosphere
$O(^1D)$	Stratosphere
$^{17}O(^1D)$	Stratosphere
$^{18}O(^1D)$	Stratosphere
O_2	Stratosphere
$O^{17}O$	Stratosphere
$O^{18}O$	Stratosphere
CO_2	Stratosphere
$CO^{17}O$	Stratosphere
$CO^{18}O$	Stratosphere
O_3	Stratosphere
$OO^{17}O$	Stratosphere
$OO^{18}O$	Stratosphere
O_2	Troposphere
$O^{18}O$	Troposphere
$O^{17}O$	Troposphere
CO_2	Troposphere
$CO^{18}O$	Troposphere
$CO^{17}O$	Troposphere
[O]	Biosphere
$[^{18}O]$	Biosphere
$[^{17}O]$	Biosphere
[O]	Geosphere
$[^{18}O]$	Geosphere
$[^{17}O]$	Geosphere

3. MODEL FOR $\Delta^{17}O$ O_2 BUDGET

3.1. Overview

The model presented here for the $\Delta'^{17}O$ budget of atmospheric O_2 consists of four reservoirs, or boxes (Fig. 2). The boxes comprise the "geosphere" (rock), the biosphere/hydrosphere with an effectively infinite supply of water (ocean and meteoric), the troposphere, and the stratosphere. The basic flows between the boxes are shown in Fig. 2. The $\Delta'^{17}O$ of atmospheric O_2 is controlled by a balance between mass fractionation associated with respiration and photosynthesis (GPP and net primary production, NPP), and sequestration of the high $\Delta'^{17}O$ in stratospheric CO_2 by isotope exchange between CO_2 and H_2O at ground level. We therefore require rates of respiration and photosynthesis, rates of CO_2 formation and loss, rates of relevant reactions involving oxygen in the stratosphere, rates of isotope exchange between CO_2 and atomic oxygen in the stratosphere, rates of mixing between the stratosphere and troposphere, and rates of oxygen isotope exchange at ground level. The rates required for this model have been determined in the past, and sub-systems of this model have been investigated in previous work (Luz et al., 1999; Liang et al., 2007; Cao and Bao, 2013). But the combination of stratosphere chemistry, stratosphere/troposphere mixing, and ground-level reaction rates have seldom, if ever, been combined in a single calculation to investigate their interactions and their capacity to match observations in concert.

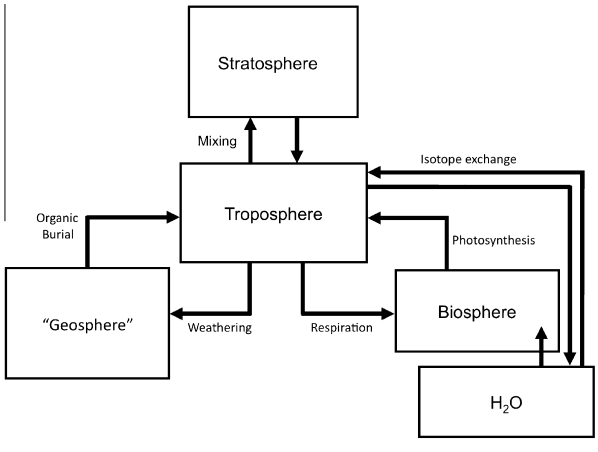

Fig. 2. Schematic illustration of the box model used in this study. Arrows depict fluxes between reservoirs. Transfer between geosphere and hydrosphere occurs on 10^8 year timescales and is too slow to be considered here. Biosphere and H_2O comprise a single box mathematically. The complete model is composed of 27 ODEs.

A successful model built upon the rates described above will be capable of explaining the mixing ratios of O_2, stratospheric and tropospheric CO_2, and stratospheric O_3, the $\delta^{18}O$ of O_2 and the $\delta^{18}O$ and $\delta^{17}O$ of stratospheric O_3, stratospheric CO_2, and tropospheric CO_2 as well as the $\Delta'^{17}O$ CO_2 flux from the stratosphere to the troposphere (‰ moles/year). These are all quantities for which we have solid observations. The model will then yield a prediction for the $\Delta'^{17}O$ atmospheric O_2 relative to a fixed and independent isotopic reference.

3.2. Stratosphere chemistry

The reaction network used in our model includes 53 reactions describing stratosphere oxygen chemistry. These reactions are described here.

An important component of the ^{17}O deficit in atmospheric O_2 comes from sequestering a ^{17}O excess produced during ozone formation in the stratosphere via exchange with CO_2, transport of CO_2 to the troposphere, and isotopic exchange between CO_2 and water at ground level (Yung et al., 1991; Bender et al., 1994). The exchange occurs between an excited state of atomic oxygen, $O(^1D)$, and CO_2 in the stratosphere. The $O(^1D)$ is a photodissociation product of stratospheric O_3. This component of O_2 $\Delta'^{17}O$ is therefore intimately associated with the kinetics of ozone formation and destruction (the Chapman cycle).

Table 1 lists the species considered in the stratosphere reaction network together with all species comprising the model. We consider ^{16}O and singly-substituted ^{18}O and ^{17}O-isotopologues of all species. We do not track the isotopomers of each isotopologue separately (so that $O^{17}O$ represents $^{17}O^{16}O + {}^{16}O^{17}O$, etc.). Symmetry numbers are accounted for in the isotope ratios (e.g., $^{34}O_2/^{32}O_2 = 2\,^{18}O/^{16}O$). The list of reactions and associated rate constants is given in Table 2. Rate constants are taken mainly from Sander et al. (2006). Where there are temperature (T), actinic flux, or number-density (n) dependencies, we use conditions at 25 km as "typical" for our stratosphere box (e.g., $T = 220$ K and $n = 8.3 \times 10^{17}$ cm^{-3}). We do this because the peak in O_3 production typically occurs at ~25 km and the column density of stratospheric air between 10 and 25 km is $\sim 0.5 \times 10^{25}$ cm^{-2} while it is only $\sim 0.05 \times 10^{25}$ between 25 and 40 km; most of the mass of ozone in the stratosphere is at altitudes near ~25 km. While this is an approximation, and there is a great deal of variability in the chemistry at greater altitude (Liang et al., 2006), the influence of this chemistry on the *bulk* isotopic composition of atomic oxygen and stratospheric CO_2 delivered to the troposphere is limited (Liang et al., 2008; Wiegel et al., 2013).

Cycling of oxygen between O_2, O_3, O (we will use O to represent $O(^3P)$), and $O(^1D)$ begins with O_2 photolysis to liberate atomic oxygen:

$$O_2 + h\nu \rightarrow O + O \quad \text{(R1a)}$$

$$O^{17}O + h\nu \rightarrow O + {}^{17}O \quad \text{(R1b)}$$

$$O^{18}O + h\nu \rightarrow O + {}^{18}O. \quad \text{(R1c)}$$

The rate constant for reactions R1 was evaluated using the expression

$$J = \int_\lambda \sigma(\lambda)\phi(\lambda)\, f(\lambda)\, d\lambda \quad (24)$$

where $\sigma(\lambda)$ is the absorption cross-section (cm^2), $\varphi(\lambda)$ is the quantum yield (assumed to be unity for R1), and $f(\lambda)$ is the actinic flux (cm^{-2} s^{-1}). We evaluated Eq. (24) using absorption cross section data from Sander et al. (2006) and a "typical" actinic flux for an altitude of ~25 km at a 30° solar zenith angle from DeMore et al. (1997) (Table 2).

The ozone formation reactions are the dominant source of mass-independent fractionation (MIF) of oxygen isotopes in the atmosphere and the only source of MIF effects in the reaction network used here. The reactions are

$$O + O_2 \xrightarrow{M} O_3 \quad \text{(R2a)}$$

$${}^{18}O + O_2 \xrightarrow{M} {}^{18}OOO \quad \text{(R2b)}$$

$${}^{17}O + O_2 \xrightarrow{M} {}^{17}OOO \quad \text{(R2c)}$$

$$O + O^{18}O \xrightarrow{M} {}^{18}OOO \quad \text{(R2d)}$$

$$O + O^{17}O \xrightarrow{M} {}^{17}OOO \quad \text{(R2e)}$$

where M represents unspecified collision partners. Because we do not track isotopomers explicitly, we point out that R2d, for example, is actually

$$O + O^{18}O \xrightarrow{M} OO^{18}O$$
$$\xrightarrow{M} O^{18}OO$$

and the isotopometric equivalents of these reactions, with subequal branching ratios (Janssen et al., 1999). Implications of this distinction on isotope-specific reactions rates are described below.

Studies that model the isotopic composition of stratospheric ozone generally focus on the MIF effect alone (Lyons, 2001; Liang et al., 2006). Our goal is to reproduce the observed isotopic compositions in the stratosphere in order to characterize the influence of the stratosphere on tropospheric O_2. Our focus is on reproducing the triple-oxygen isotopic composition of ozone and its rate of formation and destruction. We are not as concerned with the relative abundances of the asymmetric and symmetric isotopomers of O_3, for example. There is abundant evidence that ozone formation is an "end-on" process in which the MIF effect is confined mainly, if not exclusively, to the asymmetric isotopomers (Michalski and Bhattacharya, 2009). But our concern is with the bulk enrichments in $^{50}O_3$ ($^{16}O^{16}O^{18}O + {}^{18}O^{16}O^{16}O + {}^{16}O^{18}O^{16}O$) and $^{49}O_3$ ($^{16}O^{16}O^{17}O + {}^{17}O^{16}O^{16}O + {}^{16}O^{17}O^{16}O$) relative to $^{48}O_3$. Studies that track only the mass-independent fractionation effects have tended to overestimate $\Delta^{17}O$ relative to measured stratospheric values. For example, Krankowsky et al. (2007) present data for stratosphere samples obtained at or below 25 km (peak in O_3 concentrations) with mean $\delta^{17}O'$, $\delta^{18}O'$, and $\Delta'^{17}O$ values of 77 ± 10 (1σ)‰, 94 ± 13‰, and 29 ± 4‰, respectively (note the transformation from δ reported by these authors to the logarithmic δ′ values relative to SMOW cited here). Lyons (2001)

Table 2
Rate constants and rates for basic model. Constants apply to 220 K unless otherwise specified.

R1a	$O_2 + h\nu \rightarrow O + O$	$J_{R1a} = 1.109 \times 10^{-12}\ s^{-1}$	a
R1b	$O^{17}O + h\nu \rightarrow O + {}^{17}O$	$k_{R1b} = J_{R1a}$	
R1c	$O^{18}O + h\nu \rightarrow O + {}^{18}O$	$k_{R1b} = J_{R1a}$	
R2a	$O + O_2 \xrightarrow{M} O_3$	$k_{R2a} = 1.26 \times 10^{-33} \times 8.3 \times 10^{17}\ cm^3\ s^{-1}$	b
R2b	${}^{18}O + O_2 \xrightarrow{M} {}^{18}OOO$	$k_{R2b} = k_{R2a}\sqrt{\mu_{O+O_2}/\mu_{{}^{18}O+O_2}}\,\alpha_{MIF}$	
R2c	${}^{17}O + O_2 \xrightarrow{M} {}^{17}OOO$	$k_{R2c} = k_{R2a}\sqrt{\mu_{O+O_2}/\mu_{{}^{17}O+O_2}}\,\alpha_{MIF}$	
R2d	$O + O^{18}O \xrightarrow{M} {}^{18}OOO$	$k_{R2d} = k_{R2a}\sqrt{\mu_{O+O_2}/\mu_{O+O^{18}O}}\,\alpha_{MIF}$	
R2e	$O + O^{17}O \xrightarrow{M} {}^{17}OOO$	$k_{R2d} = k_{R2a}\sqrt{\mu_{O+O_2}/\mu_{O+O^{17}O}}\,\alpha_{MIF}$	
R3a	$O_3 + h\nu \rightarrow O_2 + O$	$J_{R3a} = 2.96 \times 10^{-4}\ s^{-1}$	
R3b	$OO^{18}O + h\nu \rightarrow O_2 + {}^{18}O$	$k_{R3b} = 1/3 J_{R3a}$	c
R3c	$OO^{18}O + h\nu \rightarrow O^{18}O + O$	$k_{R3c} = 2/3 J_{R3a}$	c
R3d	$OO^{17}O + h\nu \rightarrow O_2 + {}^{17}O$	$k_{R3d} = 1/3 J_{R3a}$	c
R3e	$OO^{17}O + h\nu \rightarrow O^{17}O + O$	$k_{R3e} = 2/3 J_{R3a}$	c
R3f	$O_3 + h\nu \rightarrow O_2 + O(^1D)$	$J_{R3f} = 5.01 \times 10^{-4}\ s^{-1}$	
R3g	$OO^{18}O + h\nu \rightarrow O_2 + {}^{18}O(^1D)$	$k_{R3g} = 1/3 J_{R3f}$	
R3h	$OO^{18}O + h\nu \rightarrow O^{18}O + O(^1D)$	$k_{R3h} = 2/3 J_{R3f}$	
R3i	$OO^{17}O + h\nu \rightarrow O_2 + {}^{17}O(^1D)$	$k_{R3i} = 1/3 J_{R3f}$	
R3j	$OO^{17}O + h\nu \rightarrow O^{17}O + O(^1D)$	$k_{R3j} = 2/3 J_{R3f}$	
R4a	$O_3 + O \rightarrow O_2 + O_2$	$k_{R4a} = 6.86 \times 10^{-15}\ cm^3\ s^{-1}$	
R4b	$OO^{18}O + O \rightarrow O_2 + O^{18}O$	$k_{R4b} = k_{R4a}\sqrt{\mu_{O_3+O}/\mu_{OO^{18}O+O}}$	
R4c	$OO^{17}O + O \rightarrow O_2 + O^{17}O$	$k_{R4c} = k_{R4a}\sqrt{\mu_{O_3+O}/\mu_{OO^{17}O+O}}$	
R4d	$O_3 + {}^{18}O \rightarrow O_2 + O^{18}O$	$k_{R4d} = k_{R4a}\sqrt{\mu_{O_3+O}/\mu_{O_3+{}^{18}O}}$	
R4e	$O_3 + {}^{17}O \rightarrow O_2 + O^{17}O$	$k_{R4e} = k_{R4a}\sqrt{\mu_{O_3+O}/\mu_{O_3+{}^{17}O}}$	
R4f	$O_3 + O(^1D) \rightarrow O_2 + O_2$	$k_{R4f} = 1.20 \times 10^{-10}\ cm^3\ s^{-1}$	
R4g	$OO^{18}O + O(^1D) \rightarrow O_2 + O^{18}O$	$k_{R4g} = k_{R4f}\sqrt{\mu_{O_3+O(^1D)}/\mu_{OO^{18}O+O)^1D)}}$	
R4h	$OO^{17}O + O(^1D) \rightarrow O_2 + O^{17}O$	$k_{R4h} = k_{R4f}\sqrt{\mu_{O_3+O(^1D)}/\mu_{OO^{17}O+O(^1D)}}$	
R4i	$O_3 + {}^{18}O(^1D) \rightarrow O_2 + O^{18}O$	$k_{R4i} = k_{R4f}\sqrt{\mu_{O_3+O(^1D)}/\mu_{O_3+{}^{18}O(^1D)}}$	
R4j	$O_3 + {}^{17}O(^1D) \rightarrow O_2 + O^{17}O$	$k_{R4j} = k_{R4f}\sqrt{\mu_{O_3+O(^1D)}/\mu_{O_3+{}^{17}O(^1D)}}$	
R4k	$O_3 + O(^1D) \rightarrow O_2 + O + O$	$k_{R4k} = k_{R4f}$	
R4l	$OO^{18}O + O(^1D) \rightarrow O_2 + O + {}^{18}O$	$k_{R4l} = 1/2\ k_{R4f}\sqrt{\mu_{O_3+O(^1D)}/\mu_{OO^{18}O+O(^1D)}}$	
R4 m	$OO^{18}O + O(^1D) \rightarrow O^{18}O + O + O$	$k_{R4m} = 1/2 k_{R4f}\sqrt{\mu_{O_3+O(^1D)}/\mu_{OO^{18}O+O(^1D)}}$	
R4n	$OO^{17}O + O(^1D) \rightarrow O_2 + O + {}^{17}O$	$k_{R4n} = 1/2 k_{R4f}\sqrt{\mu_{O_3+O(^1D)}/\mu_{OO^{17}O+O(^1D)}}$	
R4o	$OO^{17}O + O(^1D) \rightarrow O^{17}O + O + O$	$k_{R4o} = 1/2 k_{R4f}\sqrt{\mu_{O_3+O(^1D)}/\mu_{OO^{17}O+O(^1D)}}$	
R4p	$O_3 + {}^{18}O(^1D) \rightarrow O_2 + O + {}^{18}O$	$k_{R4p} = 1/2 k_{R4f}\sqrt{\mu_{O_3+O(^1D)}/\mu_{O_3+{}^{18}O(^1D)}}$	
R4q	$O_3 + {}^{18}O(^1D) \rightarrow O^{18}O + O + O$	$k_{R4q} = 1/2\ k_{R4f}\sqrt{\mu_{O_3+O(^1D)}/\mu_{O_3+{}^{18}O(^1D)}}$	
R4r	$O_3 + {}^{17}O(^1D) \rightarrow O_2 + O + {}^{17}O$	$k_{R4r} = 1/2 k_{R4f}\sqrt{\mu_{O_3+O(^1D)}/\mu_{O_3+{}^{17}O(^1D)}}$	
R4s	$O_3 + {}^{17}O(^1D) \rightarrow O^{17}O + O + O$	$k_{R4s} = 1/2 k_{R4f}\sqrt{\mu_{O_3+O(^1D)}/\mu_{O_3+{}^{17}O(^1D)}}$	
R5a	$M + O(^1D) \rightarrow M + O$	$k_{R5a} = 1.4 \times 10^{-10}\ cm^3\ s^{-1}$	d
R5b	$M + {}^{18}O(^1D) \rightarrow M + {}^{18}O$	$k_{5b} = k_{5a}$	
R5c	$M + {}^{17}O(^1D) \rightarrow M + {}^{17}O$	$k_{5c} = k_{5a}$	
R6a	$O_2 + {}^{18}O \rightarrow O^{18}O + O$	$k_{R6a} = k_{R6}\sqrt{\mu_{O_2+O}/\mu_{O_2+{}^{18}O}}$, $k_{R6} = 2.0x10^{-16} cm^3 s^{-1}$	
R6b	$O^{18}O + O \rightarrow O_2 + {}^{18}O$	$k_{R6b} = 1/2 k_{R6}\sqrt{\mu_{O_2+O}/\mu_{O^{18}O+O}}$	
R6c	$O_2 + {}^{17}O \rightarrow O^{17}O + O$	$k_{R6c} = k_{R6}\sqrt{\mu_{O_2+O}/\mu_{O_2+{}^{17}O}}$	
R6d	$O^{17}O + O \rightarrow O_2 + {}^{17}O$	$k_{R6d} = 1/2 k_{R6}\sqrt{\mu_{O_2+O}/\mu_{O^{17}O+O}}$	
R7a	$CO_2 + O(^1D) \rightarrow CO_2 + O$	$k_{R7a} = 4.46 \times 10^{-11}\ cm^3\ s^{-1}$	
R7b	$CO_2 + {}^{18}O(^1D) \rightarrow CO_2 + {}^{18}O$	$k_{R7b} = 1/2 k_{R7a}\sqrt{\mu_{CO_2+O(^1D)}/\mu_{CO_2+{}^{18}O(^1D)}}$	

R7c	$CO_2 + {}^{18}O({}^1D) \rightarrow CO^{18}O + O$	$k_{R7c} = 1/2 k_{R7a}\sqrt{\mu_{CO_2+O(^1D)}/\mu_{CO_2+{}^{18}O(^1D)}}$	
R7d	$CO^{18}O + O({}^1D) \rightarrow CO_2 + {}^{18}O$	$k_{R7d} = 1/2\, k_{R7a}\sqrt{\mu_{CO_2+O(^1D)}/\mu_{CO^{18}O+O(^1D)}}$	
R7e	$CO^{18}O + O({}^1D) \rightarrow CO^{18}O + O$	$k_{R7e} = 1/2 k_{R7a}\sqrt{\mu_{CO_2+O(^1D)}/\mu_{CO^{18}O+O(^1D)}}$	
R7f	$CO_2 + {}^{17}O({}^1D) \rightarrow CO_2 + {}^{17}O$	$k_{R7f} = 1/2 k_{R7a}\sqrt{\mu_{CO_2+O(^1D)}/\mu_{CO_2+{}^{17}O(^1D)}}$	
R7g	$CO_2 + {}^{17}O({}^1D) \rightarrow CO^{17}O + O$	$k_{R7g} = 1/2 k_{R7a}\sqrt{\mu_{CO_2+O(^1D)}/\mu_{CO_2+{}^{17}O(^1D)}}$	
R7h	$CO^{17}O + O({}^1D) \rightarrow CO_2 + {}^{17}O$	$k_{R7h} = 1/2 k_{R7a}\sqrt{\mu_{CO_2+O(^1D)}/\mu_{CO^{17}O+O(^1D)}}$	
R7i	$CO^{17}O + O({}^1D) \rightarrow CO^{17}O + O$	$k_{R7i} = 1/2 k_{R7a}\sqrt{\mu_{CO_2+O(^1D)}/\mu_{CO^{17}O+O(^1D)}}$	
R8a	$CO_2 + H_2^{18}O \rightarrow CO^{18}O + H_2O$	$k_{R8a} = k_{R8b}\alpha_{CO_2/H_2O}(1.00525^{18}R_{SMOW})$	e
R8b	$CO^{18}O + H_2O \rightarrow CO_2 + H_2^{18}O$	$k_{R8b} = 1.0\ \text{year}^{-1}$	f
R8c	$CO_2 + H_2^{17}O \rightarrow CO^{17}O + H_2O$	$k_{R8c} = k_{R8b}(\alpha_{CO_2/H_2O})^{\beta}(1.00525^{\beta 17}R_{SMOW})$	e
R8d	$CO^{17}O + H_2O \rightarrow CO_2 + H_2^{17}O$	$k_{R8d} = k_{R8b}$	
	CO_2–H_2O $^{18}O/^{16}O$ equilibrium	$\alpha_{CO_2/H_2O} = 1.041$	
	CO_2–H_2O $^{17}O/^{16}O$ equilibrium	$(\alpha_{CO_2/H_2O})^{0.528}$	
	Respiration rate constant	$k_r = 0.0008\ \text{year}^{-1}$	
	$^{18}O/^{16}O$ respiration fractionation	$\alpha_r = 1/1.0182$	
	$^{17}O/^{16}O$ respiration fractionation	$1/(\alpha_r)^{0.5149}$	
	Evapotranspiration $^{18}O/^{16}O$ fractionation	1.00525	
	Evapotranspiration $^{17}O/^{16}O$ fractionation	$1.00525^{0.520}$	
	O_2 weathering rate constant	$k_{O2\text{-}w} = 6.0 \times 10^{-7}\ \text{year}^{-1}$	g
	Organic burial rate constant	$k_{org} = 5.0 \times 10^{-5}\ \text{year}^{-1}$	g
	Moles stratosphere	1.8×10^{19} moles	
	Stratosphere → troposphere transport rate constant	$k_{ST} = 1.0\ \text{year}^{-1}$	h
	Moles troposphere	1.8×10^{20} moles	
	Troposphere → stratosphere transport rate constant	$k_{TS} = 0.1\ \text{year}^{-1}$	
	CO_2 weathering rate constant	$k_w = 0.000208\ \text{year}^{-1}$	i
	Rate of volcanic CO_2 emission	$f_V = 4.0 \times 10^{12}$ moles year^{-1}	j
	Rate of CO_2 effusion from oceans	$f_O = 5.88 \times 10^{15}$ moles year^{-1}	j
	CO_2 infusion to oceans rate constant	$k_A = 0.1172\ \text{year}^{-1}$	j

a: Stratosphere rate constants from Sander et al. (2006) unless otherwise specified.
b: The second term is the number density at 25 km in cm^{-3}.
c: 1/3 corrects rate for reactant OOQ = OOQ + OQO + QOO, Q = ^{18}O or ^{17}O. 2/3 corrects for product OQ = OQ + QO.
d: Adjusted from $k = 2.93 \times 10^{-11}$ so that [M] = [N_2] + [O_2] at steady-state [O_2] and k [O_2] = k_{5a} [M].
e: 1.00525 corrects for the isotopic composition of evapotranspiration. $^iR_{SMOW} = {}^iO/{}^{16}O$ SMOW. This formulation accounts for an effectively infinite water reservoir.
f: Welp et al. (2011).
g: Lasaga and Ohmoto (2002).
h: Appenzeller and Holton (1996).
i: Kump et al. (2000). Isotopologue rate constants obtained by multiplying by $^{18}R_{SMOW}$ or $^{17}R_{SMOW}$.
j: Solomon et al. (2007). Rate constants for singly-substituted isotopologues are obtained by multiplying by $^{18}R_{SMOW}$ or $^{17}R_{SMOW}$.

obtained model $\Delta'^{17}O$ values of ~40‰ for bulk O_3 using earlier published rate constants (Morton et al., 1990; Mauersberger et al., 1999). In that work the asymmetric species OOQ (where Q = ^{17}O or ^{18}O) were computed to have $\Delta'^{17}O$ values of ~85‰ balanced by strongly negative $\Delta'^{17}O$ values of ~ −50‰ for the symmetric OQO species. Liang et al. (2006) used rate constants based on the η effect of Gao and Marcus (2002) applied to stratospheric conditions to arrive at $\delta'^{17}O$, $\delta'^{18}O$, and $\Delta'^{17}O$ values of 82‰, 86‰, and 39‰, respectively, at ~25 km with $\Delta'^{17}O$ for the asymmetric OOQ isotopomers and symmetric OQO isotopomers of 58‰ and ~0‰, respectively. In both cases, regardless of the different results for the asymmetric species, the overestimates of between 7 and >10‰ in bulk ozone $\Delta'^{17}O$ would bias our results for the purpose at hand.

An alternative phenomenological approach, and the one adopted here, is to consider that the isotope effects associated with reactions R2 derive from a convolution of mass-dependent (MD) components and a purely MIF component (Mauersberger et al., 1999). The most straightforward way of expressing the total effect is therefore as a product of the mass-dependent fractionation factor, α_{MD}, and an MIF fractionation factor, α_{MIF}. The fractionation factor is the ratio of the rate constants for the isotopically-substituted reactants, k', and the non-substituted reactants, k, yielding $k'/k = \alpha = \alpha_{MD}\ \alpha_{MIF}$. The mass-dependent fractionation effect is in part due to the temperature-independent ratio of collision frequencies.

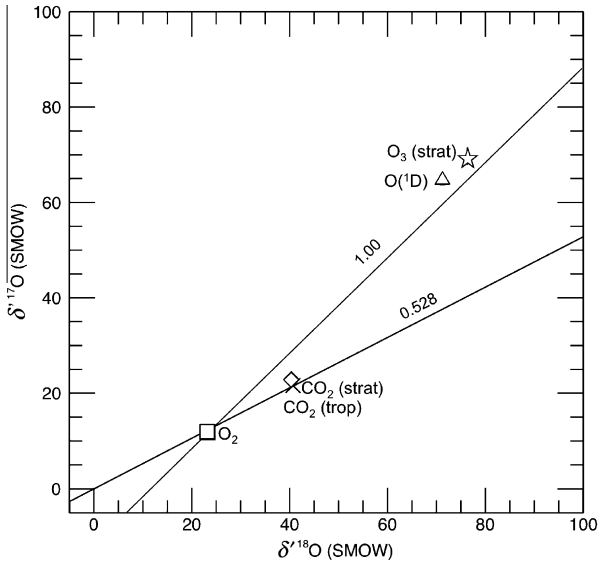

Fig. 4. Three-isotope plot ($\delta'^{i}O = 10^3\ln(\delta^{i}O/10^3 + 1)$) showing the steady-state solution to the box model using present-day rates and rate coefficients in Table 2. The two reference lines are for pure MIF relative to O_2 (slope = 1.00) and high-temperature and/or water mass fractionation (slope = 0.528).

Values for α_{MD} based on collision frequencies are obtained from the reduced masses of the isotopically-substituted reactants, μ', and the reduced mass of the reactants for the non-substituted reactants, μ:

$$\alpha_{MD} = \sqrt{\frac{\mu}{\mu'}}. \quad (25)$$

Eq. (25) is a simplification in that it ignores contributions due to vibrational frequencies for the transition state reaction coordinates and zero-point energy differences between reactant isotopologues and transition-state isotopic species. Deriving these terms for all of the relevant reactions used here is beyond the scope of the present work. We therefore apply Eq. (25) as an approximation for all relevant cases throughout the reaction network (Table 2). In the case of R2a through R2e, values for $10^3\ln(\alpha_{MD})$ vary from −5.10‰ for $(O + O^{17}O)/(O + O_2)$ to −38.57‰ for $(^{18}O + O_2)/(O + O_2)$. The remaining factor, α_{MIF}, should apply equally to both ^{17}O- and ^{18}O-products of reactions R2 by definition. The overall fractionation factor $\alpha = \alpha_{MD}\ \alpha_{MIF}$ is known to be temperature dependent, with the magnitude of the MIF correlating positively with T (Morton et al., 1990; Janssen et al., 2003; Janssen, 2005). Some of this temperature-dependence has been attributed to simultaneous exchange of oxygen isotopes between O and O_2 (Janssen et al., 2003). However, deconvolution of the effects of mass-dependent and MIF effects in measured fractionation factors for ozone formation has not been accomplished with certainty. Because collisional mass-dependent fractionation is not temperature dependent, and in the absence of a perfect understanding of the sources of $\alpha(T)$ for reactions R2, we assign the temperature-dependence in α to α_{MIF} in effect by assigning α_{MIF} a temperature-integrated, or effective, value that reproduces the observed isotopic composition of O_3 at peak mixing ratios in the stratosphere.

We find that an α_{MIF} value of 1.065, in combination with mass-dependent fractionation due to collision frequency and the reaction network summarized in Table 2, reproduces typical $\delta'^{17}O$, $\delta'^{18}O$ and $\Delta'^{17}O$ values of stratospheric O_3 at peak ozone mixing ratios within the spread of the data (Section 4). In detail, while the model and measured $\Delta'^{17}O$ values match, the model $\delta'^{18}O$ is low by ~10‰ compared with the mean measured $\delta'^{18}O$ for O_3. We attribute this offset to the approximation (Eq. (25)) used for the mass-dependent fractionation factors. The convolution of the α_{MIF} with the mass-dependent collision frequency fractionation gives a total fractionation factor α (i.e., k'/k) for product $^{50}O_3/^{48}O_3$ of 1.044 that compares favorably with the value of 1.041 for the same parameter at 220 K reported by Janssen (2005) (obtained by averaging the values of 0.838 and 1.244 for the $^{18}O + O_2$ and $O + O^{18}O$ reactions, respectively).

Photolysis of O_3 with high $\Delta^{17}O$ values releases atomic oxygen with a high $\Delta'^{17}O$ signature that is central to the O_2 $\Delta^{17}O$ budget. The reactions are

$$O_3 + h\nu \rightarrow O_2 + O \quad (R3a)$$
$$OO^{18}O + h\nu \rightarrow O_2 + {}^{18}O \quad (R3b)$$
$$OO^{18}O + h\nu \rightarrow O^{18}O + O \quad (R3c)$$
$$OO^{17}O + h\nu \rightarrow O_2 + {}^{17}O \quad (R3d)$$
$$OO^{17}O + h\nu \rightarrow O^{17}O + O \quad (R3e)$$
$$O_3 + h\nu \rightarrow O_2 + O(^1D) \quad (R3f)$$
$$OO^{18}O + h\nu \rightarrow O_2 + {}^{18}O(^1D) \quad (R3g)$$
$$OO^{18}O + h\nu \rightarrow O^{18}O + O(^1D) \quad (R3h)$$
$$OO^{17}O + h\nu \rightarrow O_2 + {}^{17}O(^1D) \quad (R3i)$$
$$OO^{17}O + h\nu \rightarrow O^{17}O + O(^1D). \quad (R3j)$$

The quantum yields for the O and $O(^1D)$ products are taken from Matsumi and Kawasaki (2003) where it is assumed that $\varphi_{1D}(\lambda) + \varphi_{O}(\lambda) = 1$. In this formulation $\varphi_{1D}(\lambda)$ has values of 0.9 for $\lambda < 306$ nm and 0.0 for $\lambda > 340$ nm. We evaluated the photodissociation rate constants for R3a–R3j using Eq. (24), the absorption cross section data from Sander et al. (2006) and the same "typical" actinix flux for an altitude of ~25 km used for O_2 photolysis. The rate constant J (s^{-1}) for R3a vs. wavelength is shown in Fig. 4 and the integrated values and isotopic equivalents are tabulated in Table 2

Destruction of O_3 isotopologues occurs by reaction with atomic oxygen (as well as by catalytic cycles discussed in Section 4.1). The reaction network used here includes 19 such reactions involving O_3, $OO^{18}O$, $OO^{17}O$, O, $O(^1D)$, ^{18}O, ^{17}O, $^{18}O(^1D)$ and $^{17}O(^1D)$ as reactants (Table 2). The reactions are of the form

$$O_3 + O \rightarrow O_2 + O_2. \quad (R4)$$

Because $O(^1D)$ is the primary carrier of the positive $\Delta^{17}O$ produced by ozone formation via exchange with CO_2 in the stratosphere, the residence time of this excited

state of atomic oxygen is important to the budget for $\Delta'^{17}O$ O_2. Quenching of $O(^1D)$ to O is included with the reactions

$$M + O(^1D) \rightarrow M + O \quad (R5a)$$

$$M + {}^{18}O(^1D) \rightarrow M + {}^{18}O \quad (R5b)$$

$$M + {}^{17}O(^1D) \rightarrow M + {}^{17}O \quad (R5c)$$

where M is a collision partner, dominantly N_2 and O_2.

Oxygen isotope exchange between atomic oxygen and molecular oxygen is another important facet of determining the oxygen isotopic composition of species considered here (Janssen et al., 2003). We include oxygen isotope exchange using

$$O_2 + {}^{18}O \rightarrow O^{18}O + O \quad (R6a)$$

$$O^{18}O + O \rightarrow O_2 + {}^{18}O \quad (R6b)$$

$$O_2 + {}^{17}O \rightarrow O^{17}O + O \quad (R6c)$$

$$O^{17}O + O \rightarrow O_2 + {}^{17}O. \quad (R6d)$$

Lastly, quenching of $O(^1D)$ by reaction with CO_2 transfers the positive $\Delta'^{17}O$ signal to CO_2 (Yung et al., 1991) and so the rate of these reactions are included here using

$$CO_2 + O(^1D) \rightarrow CO_2 + O \quad (R7a)$$

$$CO_2 + {}^{18}O(^1D) \rightarrow CO_2 + {}^{18}O \quad (R7b)$$

$$CO_2 + {}^{18}O(^1D) \rightarrow CO^{18}O + O \quad (R7c)$$

$$CO^{18}O + O(^1D) \rightarrow CO_2 + {}^{18}O \quad (R7d)$$

$$CO^{18}O + O(^1D) \rightarrow CO^{18}O + O \quad (R7e)$$

$$CO_2 + {}^{17}O(^1D) \rightarrow CO_2 + {}^{17}O \quad (R7f)$$

$$CO_2 + {}^{17}O(^1D) \rightarrow CO^{17}O + O \quad (R7g)$$

$$CO^{17}O + O(^1D) \rightarrow CO_2 + {}^{17}O \quad (R7h)$$

$$CO^{17}O + O(^1D) \rightarrow CO^{17}O + O. \quad (R7i)$$

With this reaction network for the model stratosphere the all-important rate equation for the time-dependent abundance of $O(^1D)$, $n_{O(1D)}$, is

$$\begin{aligned}\frac{dn^{\mathrm{Strat}}_{O(^1D)}}{dt} &= J_{R3f} n_{O_3} + k_{R3h} n_{OO^{18}O} + k_{R3j} n_{OO^{17}O} - n_{O(^1D)} \\ &\times (k_{R4g} n_{OO^{18}O} k_{R4h} n_{OO^{17}O} + k_{R4k} n_{O_3} + k_{R4l} n_{OO^{18}O} \\ &+ k_{R4m} n_{OO^{18}O} + k_{R4n} n_{OO^{17}O} + k_{R4o} n_{OO^{17}O} + k_{R5a} n_M \\ &+ k_{R7a} n_{CO_2} + k_{R7d} n_{CO^{18}O} + k_{R7e} n_{CO^{18}O} + k_{R7g} n_{CO^{17}O} \\ &+ k_{R7i} n_{CO^{17}O})\end{aligned} \quad (26)$$

where the rate constants k and J have subscripts tied to the reactions as listed in the text and in Table 2 and all molar abundances n_i refer to the stratosphere. Eq. (26) and its isotopic equivalents show that the rates of formation and destruction of O_3 isotopologues and the rate of quenching by collisions together control the abundance and isotopic composition of $O(^1D)$ and therefore $\Delta'^{17}O$ of stratospheric CO_2 (reactions R7b–R7i). The $\Delta'^{17}O$ budget of O_2 depends in part on the balance depicted in Eq. (26).

Rate constants listed in Table 2 are shown in the usual units ($cm^3\ s^{-1}$ for second-order reactions). In order to combine equations like Eq. (26) with fluxes in our model, we convert k values from $cm^3\ s^{-1}$ to moles $year^{-1}$ by multiplying by (s/year) L/V where L is Avogadro's number and V is the volume of the stratosphere. For $V = 2.8 \times 10^{25}$ cm^3, $L/V = 0.0215$ molecules cm^{-3}.

3.3. Stratosphere-troposphere mixing

The flux of CO_2 downward across the tropopause determines the rate of CO_2 $\Delta'^{17}O$ transport from the stratosphere to the troposphere and eventually to ground level. We use a stratosphere–troposphere transport rate of 6.8×10^{17} kg $year^{-1}$, or 2.4×10^{19} moles $year^{-1}$ (Appenzeller and Holton, 1996). The mass of the stratosphere is 5.2×10^{17} kg and the average molecular mass is 4.8×10^{-26} kg/molecule, yielding 1.8×10^{19} moles of air in our model stratosphere with volume V. We treat the mixing between stratosphere and troposphere as first-order rate equations. Dividing the moles of air by the flux rate above yields a first-order rate constant for stratosphere-to-troposphere mixing, k_{ST}, of 1 $year^{-1}$ (residence time of 1 year). This value is likely accurate to a factor of ~2. The troposphere consists of $\sim 1.8 \times 10^{20}$ moles air. Continuity therefore requires a troposphere-to-stratosphere mixing rate constant, k_{TS}, of 0.1 $year^{-1}$ (residence time of 10 years). These values are consistent with post-bomb ^{90}Sr stratosphere and troposphere residence times (Fabian et al., 1968).

3.4. Respiration and photosynthesis

Bender et al. (1994) estimate an O_2 turnover time (e-fold time) of 1.2 kyear, corresponding to a respiration rate constant of 0.0008 $year^{-1}$. The rate of respiration is then $r_r = k_r n_{O_2}$ where k_r is the respiration rate constant. The rate of photosynthesis, r_p, is balanced against the rate of respiration to produce the observed concentration of atmospheric O_2 (21% mixing ratio). We refer to this rate when we refer to GPP in our model. Changes in net primary production (NPP) would constitute a change in r_p/k_r and a change in O_2 mixing ratio (e.g., Eq. (17)). We vary GPP for illustration purposes at fixed NPP in this work unless otherwise specified.

Using the weightings of respiration pathways discussed above (Angert et al., 2003) and isotopic discriminations for these pathways from Nagel et al. (2001) and Guy et al. (1993), we obtain an overall isotopic fractionation for respiration of 18‰. We apply the fractionation by multiplying k_r by $\alpha_r = 1/(1.0182)$ for $O^{18}O$ consumption and $1/(1.0182^{\beta})$ for $O^{17}O$ uptake (Table 2). As discussed previously, we use a nominal β for respiration of 0.5149.

For photosynthesis we consider an average source water that includes a fraction of water enriched in ^{18}O relative to ^{16}O due to evapotranspiration. A global average water $\delta'^{18}O$ (SMOW) of 5.25‰ in combination with the 18‰ due to respiration produces the observed $\delta^{18}O$ of air O_2. We specify this enrichment in the source water by multiplying the photosynthesis rate constant for O_2 production by 1.00525 for $O^{18}O$ and $1.00525^{\beta water}$ for $O^{17}O$ (Table 2). Evapotranspiration includes evaporation and diffusion, both with intrinsic β values of ~0.513 (e.g., Young et al.,

2002). The value for β_{water} indicated by the leaf transpiration data of Landais et al. (2006) is higher at 0.519 based on direct measurements with humidities of 30–40%. Terrestrial water accounts for ~60% of gross primary production with the remaining fraction coming from oceans (Angert et al., 2004; Hoffman et al., 2004). Mixing leaf water with ocean water in these proportions to achieve the specified global average water source leads to a global β_{water} of 0.519, indistinguishable from the transpiration value. Recent work by Barkan and Luz (2011) suggests that photosynthesis in marine environments could be associated with a fractionation of 2.9‰ in $\delta'^{18}O$ with an associated effective β_{water} of 0.525. Ascribing this fractionation to the kinetics of O_2 production from ocean waters and mixing this fractionated source of O_2 with the terrestrial water source to obtain the global source $\delta'^{18}O$ of 5.25‰ (i.e., $\delta'^{18}O$ leaf water = 6.825‰ and $\delta'^{18}O$ produced by ocean water = 2.883‰) raises the β_{water} slightly to 0.520 (mixing calculations are performed using isotope ratios to account for the non-linear mixing in $\delta'^{17}O$ vs $\delta'^{18}O$ space). We use this effective β_{water} of 0.520 to account for fractionation associated with water sources for photosynthesis globally.

The global source water isotopic composition also produces the correct isotopic composition of CO_2 (discussed in Section 3.5), which we take as evidence for its validity. The $\delta'^{18}O$ value for air that we use corresponds to the original (non-logarithmic) $\delta^{18}O$ (relative to SMOW) value of 23.5‰ (Kroopnick and Craig, 1972). It is lower than the value of 23.88‰ obtained by Barkan and Luz (2005). We have retained the earlier number for the time being because when our reference oxygen in our laboratory yields air O_2 at 23.5‰ we obtain 5.2‰ for San Carlos olivine, both relative to SMOW (Section 5). The San Carlos olivine value is common to many laboratories and generally agreed upon (e.g., Mattey et al., 1994). In addition, we obtain $\delta^{18}O$ values for meteorites that are comparable to those obtained at the University Chicago, a laboratory that was originally calibrated by fluorinating SMOW. Finally, Kusakabe and Matsuhisa (2008) and Tanaka and Nakamura (2012) obtained values of 5.28 ± 0.10 (1σ)‰ and 5.28 ± 0.08 (1σ)‰, respectively, for San Carlos olivine measured relative to reference gases calibrated directly by fluorination of VSMOW. If we were to adopt the higher air value of 23.9‰ our rock data would be greater than accepted values and greater than the direct comparisons between San Carlos olivine and VSMOW by 0.4‰ (~4× greater than analytical uncertainties). There is a pressing need for a single laboratory to measure mantle rocks, VSMOW, and air O_2 together to remedy this apparent closure error. Regardless, the difference between 23.5‰ and 23.9‰ for $\delta^{18}O$ of air O_2 is negligible for the purposes of the present study.

3.5. CO_2

The positive $\Delta'^{17}O$ signal acquired in reactions R7 are consumed and effectively lost to the greater mass of oxygen in the hydrosphere by isotope exchange between CO_2 carried from the stratosphere to the troposphere and water at or near ground level:

$$CO_2 + H_2{}^{18}O \rightarrow CO^{18}O + H_2O \quad \text{(R8a)}$$

$$CO^{18}O + H_2O \rightarrow CO_2 + H_2{}^{18}O \quad \text{(R8b)}$$

$$CO_2 + H_2{}^{17}O \rightarrow CO^{17}O + H_2O \quad \text{(R8c)}$$

$$CO^{17}O + H_2O \rightarrow CO_2 + H_2{}^{17}O. \quad \text{(R8d)}$$

This exchange is catalyzed enzymatically for leaf and soil waters (Francey and Tans, 1987) and is estimated to be characterized by a global e-fold timescale ($1/k_{R8b}$) of 1–2 years (Farquhar et al., 1993; Welp et al., 2011). We adopt the 1-year value of Welp et al. (2011) in the model calculations. Isotope fractionation of CO_2 by reactions R8 is due to two sources. One is the fractionation of leaf and soil waters relative to SMOW and the other is the equilibrium fractionation factor between CO_2 and H_2O. For the former we use the same globally-averaged isotopic composition of source waters for photosynthesis, $\delta'^{18}O$ (SMOW) of 5.25‰, assuming that this is the net effect of low $^{18}O/^{16}O$ in precipitation and high $^{18}O/^{16}O$ due to evaporation on leaves. For the latter we use $\alpha_{CO_2/H_2O} = 1.041$ for $^{18}O/^{16}O$, appropriate for ground-level temperatures (Beck et al., 2005). For $^{17}O/^{16}O$ we use $(\alpha_{CO_2/H_2O})^{\beta} = 1.041^{\beta}$ where $\beta = 0.528$ is a nominal value for equilibrium fractionation. A lower value for the equilibrium β of 0.525 to 0.524 (e.g., Cao and Liu, 2011) alters our final $\Delta'^{17}O$ for O_2 by $<2 \times 10^{-4}$ (<0.2 per meg). Because water is unyielding in its isotope ratios in our model, the abundances of the water isotopologues are folded into the rate constants for Reactions R8 such that in general $r_{R8} = k_{R8} n_{CO_2}$. Therefore, in order to apply these isotope effects we multiply $k_{R8b} = k_{R8d}$ by the appropriate fractionation factors and water isotopologue ratios so that $k_{R8a} = k_{R8b}\ \alpha_{CO_2/H_2O}$ ($1.00525\ ^{18}R_{SMOW}$) and $k_{R8c} = k_{R8b}\ (\alpha_{CO_2/H_2O})^{\beta}$ ($1.00525^{0.528}\ ^{17}R_{SMOW}$) (Table 2).

Atmospheric carbon dioxide is produced in our model by geological emissions (f_V, volcanoes, moles year^{-1}), release from the oceans (f_O, moles year^{-1}), and respiration. Consumption of CO_2 is by drawdown by weathering ($k_w n_{CO_2}^{Trop}$, moles year^{-1}), uptake by the oceans ($k_A n_{CO_2}^{Trop}$, moles year^{-1}), and photosynthesis. The rate of photosynthesis in the model is not linked to the atmospheric concentration of CO_2. This assumption is required by the lack of clear relationships between $[CO_2]$ and r_p on a global scale (Makino and Mae, 1999; Biswas et al., 2013; Martin et al., 2013). The example of the rate equation for CO_2 (i.e., $C^{16}O_2$) serves to illustrate the CO_2 budget in the model:

$$\frac{dn_{CO_2}^{Trop}}{dt} = f_V + f_O + k_{ST} n_{CO_2}^{Strat} + k_r n_{O_2} + k_{R8b} n_{CO^{18}O}^{Trop} + k_{R8d} n_{CO^{18}O}^{Trop} - r_p - n_{CO_2}^{Trop}(k_w + k_A + k_{R8a} + k_{R8c} + k_{TS}) \quad (27)$$

Rate constants and references relevant to Eq. (27) and those for the other isotopologues of CO_2 are given in Table 2. Most come from the IPCC (Solomon et al., 2007) and from Kump et al. (2000). For simplicity, we assume that CO_2 is produced with the oxygen isotopic ratios of SMOW, so that for $C^{18}OO$, for example, the volcanic production is $f_V\ ^{18}R_{SMOW}$. This approximation is justified by the rapid equilibration of CO_2 and H_2O that will overwhelm the majority of other effects.

3.6. Geological timescales

For completeness the model includes the longer-term components of the oxygen cycle as described by Lasaga and Ohmoto (2002). These are an O_2 weathering uptake by the geosphere and an effective O_2 production term due to organic burial (Table 2). This last term is a negative feedback (burial of organics depends on $1/n_{O_2}$) that operates on 10^5 to 10^6 year timescales. Weathering and organic burial in effect comprise a distinct eigenmode for the solutions presented here and have limited impact on the results.

Table 3
Steady-state solution for the basic model. See text for explanations of target values.

Isotope ratios	Per mil	Target values
$\delta'^{18}O$ O	51.869	
$\delta'^{18}O$ O(^{1}D)	71.107	
$\delta'^{18}O$ O_2 Str	23.212	
$\delta'^{18}O$ CO_2 Str	40.345	
$\delta'^{18}O$ O_3	76.268	94 ± 13 (1σ)
$\delta'^{18}O$ O_2 Tro	23.212	23.2
$\delta'^{18}O$ CO_2 Tro	40.688	40.2
$\delta'^{17}O$ O	26.887	
$\delta'^{17}O$ O(1D)	64.599	
$\delta'^{17}O$ O_2 Str	11.886	
$\delta'^{17}O$ CO_2 Str	22.915	
$\delta'^{17}O$ O_3	69.766	77 ± 10 (1σ)
$\delta'^{17}O$ O_2 Tro	11.887	
$\delta'^{17}O$ CO_2 Tro	21.601	
$\Delta^{17}O$ O	−0.500	
$\Delta^{17}O$ O(^{1}D)	27.054	
$\Delta^{17}O$ O_2 Str	−0.370	
$\Delta^{17}O$ CO_2 Str	1.613	1.65
$\Delta^{17}O$ O_3	29.497	29 ± 4 (1σ)
$\Delta^{17}O$ O_2 Tro	−0.410	
$\Delta^{17}O$ CO_2 Tro	0.118	
Species	Moles/mole fraction (X)	
O	1.23×10^9	
^{17}O	4.68×10^5	
^{18}O	2.64×10^6	
O(1D)	3.83×10^3	
$^{17}O(^1D)$	1.51	
$^{18}O(^1D)$	8.40	
O_2 Strat	3.80×10^{18}	
$O^{17}O$ Strat	2.85×10^{15}	
$O^{18}O$ Srat	1.59×10^{16}	
CO_2 Strat	5.29×10^{15}	
$CO^{17}O$ Strat	2.01×10^{12}	
$CO^{18}O$ Strat	1.13×10^{13}	
O_3	1.28×10^{14}	
$OO^{17}O$	1.53×10^{11}	
$OO^{18}O$	8.50×10^{11}	
O_2 Trop	3.80×10^{19}	
$O^{18}O$ Trop	1.59×10^{17}	
$O^{17}O$ Trop	2.85×10^{16}	
CO_2 Trop	5.29×10^{16}	
$CO^{18}O$ Trop	1.13×10^{14}	
$CO^{17}O$ Trop	2.00×10^{13}	
XO_2 Tro	0.212	0.21
XCO_2 Tro	2.944×10^{-4}	2.70×10^{-4}
XCO_2 Strat	2.944×10^{-4}	
XO_3 Strat	7.184×10^{-6}	2×10^{-6} to 8×10^{-6}
$\Delta^{17}CO_2$ flux	8.55×10^{15}	3.60×10^{15}

3.7. Calculation method

The 27 ordinary differential equations (ODEs) comprising the model were solved using a Fortran program built around the Livermore Solver for Ordinary Differential Equations (DLSODE) (Hindmarsh, 1983). DLSODE has the capability to solve ODEs using either a user-supplied Jacobian matrix (where the ODEs are stiff) or by estimation of the Jacobians using difference quotients. Solutions were obtained at relative accuracies of between 10^{-12} and 10^{-15} depending upon the model run. Accuracy of the $\Delta'^{17}O$ calculations was tested by setting α_{MIF} to unity and $\beta_{resp} = \beta_{water} = 0.528$. Under these conditions, the only sources of variable $\Delta'^{17}O$ are the mass-dependent fractionation factors defined by reduced masses of reactants and the effects of mixing. The steady-state $\Delta'^{17}O$ of O_2 in this fiducial calculation is 0.0097‰, the value for tropospheric CO_2 is −0.0280‰, for stratospheric CO_2 it is −0.1644‰, and for O_3 it is 0.1535‰. These values are well within the ranges expected for the reduced-mass effects on β.

4. MODEL RESULTS

4.1. Comparisons with observables

Our basic model consists of the rates and fluxes in Table 2. There are three parameters tuned to give desired results. One is r_p/k_r to give the present-day mixing ratio of O_2 in air. Another is a_{MIF} to give an appropriate $\Delta'^{17}O$ for stratospheric O_3. The last is the average $^{18}O/^{16}O$ composition of water used for photosynthesis, yielding the present-day $\delta^{18}O$ of O_2. The value we chose is reasonable, but it is tuned within limits. Results for observables other than $[O_2]$ and $\delta^{18}O$ of O_3 and O_2 can be used as measures of the success or failure of the model. Our initial condition has virtually no atmospheric O_2. We run the model for at least 600,000 years to achieve steady state. Running for 10^5 years, well beyond the turnover time for O_2, ensures that we capture all contributions of different timescales (e.g., run up to the steady state $[CO_2]$). Results for the basic model upon achieving steady state are summarized in Table 3.

A summary of our nominal isotope results obtained using the basic model is shown in three-isotope space in Fig. 4. The model reproduces the $\Delta'^{17}O$ of O_3 with a calculated value of 29.5‰ and a target value of 29‰. The steady-state $[CO_2]$ is 294 ppmv, in reasonable agreement with, although slightly higher than, pre-industrial values of ~270 ppmv. The calculated steady-state $[O_3]$ in the stratosphere is 7.2 ppmv which compares favorably to values at ~25 to 30 km of about 2–10 ppmv (Grewe, 2005). The calculated $[O_3]$ is on the high side of this range because it is well known that the Chapman cycle, in the absence of catalytic cycles involving HO_2, OH, NO, and NO_2 that destroy ozone, overestimates $[O_3]$ by a factor of ~2. It turns out that the rate of stratosphere chemistry is more important than the precise concentration of O_3 in determining $\Delta'^{17}O$ of O_2.

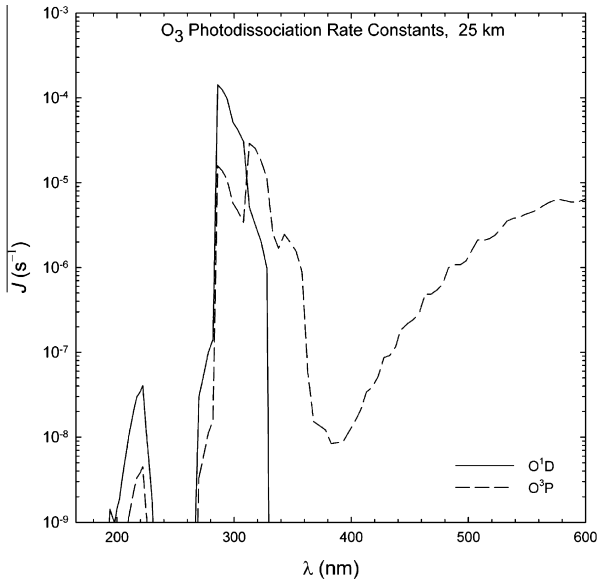

Fig. 3. Photodissociation rate consants for O_3 as a function of wavelength using an actinic flux at 25 km. The J value for the model is obtained by integrating over the values shown here. Solid line shows $O(^1D)$ channel while the dashed line is for the $O(^3P)$ channel.

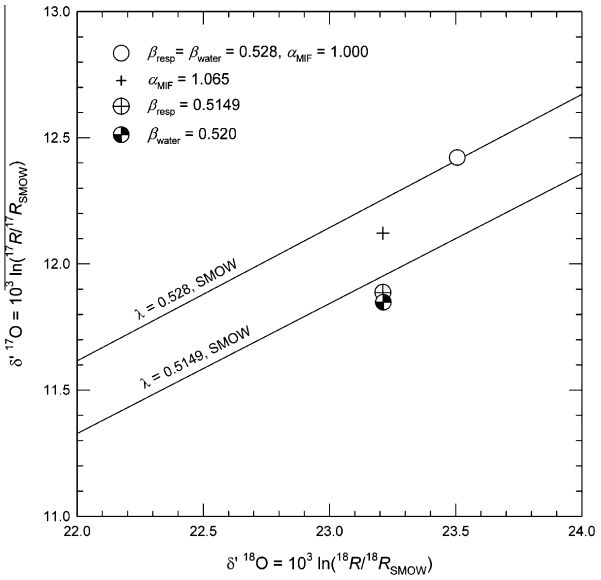

Fig. 5. Three-isotope plot showing model solutions for the case where there is no MIF fractionation associated with ozone formation and equilibrium-like fractionation exponents where $\beta_{resp} = \beta_{water} = 0.528$ (open circle); the case for $\alpha_{MIF} = 1.065$ and $\beta_{resp} = \beta_{water} = 0.528$, representing the $\Delta'^{17}O$ O_2 effect due to the stratosphere alone (cross); the case that includes both $\alpha_{MIF} = 1.065$ and $\beta_{resp} = 0.5149$, representing the effects from the stratosphere and respiration (circle with cross); and the case where $\alpha_{MIF} = 1.065$, $\beta_{resp} = 0.5149$, and $\beta_{water} = 0.520$, representing a complete model for atmospheric $\Delta'^{17}O$ O_2 (black/white circle). Fractionation lines through the origin are shown for reference.

The $\Delta^{17}O$ CO_2 flux from stratosphere to troposphere (‰ moles CO_2 $year^{-1}$) is a key factor controlling the magnitude of the stratospheric contribution to $\Delta'^{17}O$ of O_2. Boering et al. (2004) obtain an estimate for this flux of $3.6 \pm 0.9 \times 10^{15}$‰ moles CO_2 $year^{-1}$. The model returns a value at steady state of 8.6×10^{15}‰ moles CO_2 $year^{-1}$. We repeated our calculations using a lower stratosphere-to-troposphere flux of 6.9×10^{18} moles $year^{-1}$ given by Holton (1990), yielding a $\Delta'^{17}O$ CO_2 flux of 7.5×10^{15}‰ moles CO_2 $year^{-1}$. We cannot find justification for lowering the stratosphere-troposphere flux any further and so the overestimate of the CO_2 isotopic flux cannot be alleviated by altering the rate of transport from the stratosphere to the troposphere.

The $\Delta'^{17}O$ of stratospheric CO_2 also controls this isotopic flux. For comparisons with our model, we derived a bulk stratospheric $\Delta^{17}O$ of CO_2 from $\Delta^{17}O$ vs. altitude (h) data compiled by Boering et al. (2004). The data shown in their Fig. 3 were divided into 8 unequal altitude bins, Δh, and weighted by the column density for each bin using a typical number density–altitude relationship (Jacobson, 2005). The sum over all altitude intervals Δh is then used to arrive at an average $\Delta^{17}O$ for stratospheric CO_2:

$$\hat{\Delta}^{17}O\ CO_2 = \sum \Delta^{17}O\ CO_2(\Delta h)\left[\int_{\Delta h} n(h)dh \Big/ \int_{10km}^{60km} n(h)dh\right]. \quad (28)$$

Evaluation of Eq. (28) for these data gives an average $\Delta^{17}O$ CO_2 for the stratosphere of 1.65‰. Our model value is 1.61‰, which we take to be good agreement. However, the agreement is partly fortuitous. Boering et al. (2004) use a different definition for $\Delta^{17}O$ than that used here and the $\Delta'^{17}O$ (using Eq. (5) and $\beta = \lambda = 0.528$) values in this study are 0.9 times the $\Delta^{17}O$ values reported by Boering et al. for the same isotopic compositions. If converted to their approximation for $\Delta^{17}O$ our value for $\Delta^{17}O$ CO_2 becomes 1.83‰. For the same reason, our $\Delta^{17}O$ CO_2 flux becomes 9.6×10^{15}‰ moles CO_2 $year^{-1}$ using their definition. The model $\delta'^{18}O$ values for tropospheric and stratospheric CO_2 are 40.7‰ and 40.4‰, respectively, matching measured values generally between 40‰ and 43‰ (Yakir, 2003).

In summary, with the exception of a $\Delta^{17}O$ CO_2 flux that is high by approximately a factor of 2, the relevant atmospheric observables are reproduced in our basic model in which rates and fluxes have their nominal values (Table 2).

4.2. Predicted $\Delta'^{17}O$ of O_2

The model predicts that the $\Delta'^{17}O$ of O_2 relative to the water reference line with a slope λ of 0.528 is −0.410‰ at $\delta'^{18}O = 23.2$‰ (Fig. 5) as calculated using Eq. (5) where the intercept of the reference line in three-isotope space is zero by definition (the water line passes through SMOW). The contribution from the stratosphere alone is determined by running the model to steady state with $\beta_{resp} = \beta_{water} = 0.528$, matching the water reference value and so removing the effects of the respiration and evapotranspiration β values. The result is $\Delta'^{17}O = -0.134$ (Fig. 5). In other words, the model predicts that the relative contributions of

respiration + evapotranspiration and stratosphere chemistry to the total $\Delta^{17}O$ of atmospheric O_2 are 67% and 33%, respectively. The value of 134 per meg coming from the stratosphere is similar to the 120 per meg arrived at by Angert et al. (2004) and the 155 per meg originally suggested by Luz et al. (1999). Respiration accounts for 57% of the negative $\Delta^{17}O$ of atmospheric O_2 (0.235‰) and evapotranspiration fractionation comprises 10% of the overall effect (0.041‰). We consider the majority of the signal that comes from respiration to be another manifestation of the Dole effect. This conclusion contrasts with that of Bao et al. (2008). These authors conclude that 83% of the ^{17}O deficit in atmospheric O_2 is inherited from the stratosphere based on a $\Delta^{17}O$ O_2 value of −0.23‰ calculated as $\delta'^{17}O$–0.52 $\delta'^{18}O$. They derive a stratosphere component of −0.19‰ and a β_{resp} component of 0.04‰, the latter based on the difference between 0.52 and a previously published β_{eff} for respiration of 0.518 applied over 18‰ fractionation due to respiration. The slope value of 0.52 appears to be arbitrary.

The contrast in estimates of the stratospheric contributions to the $\Delta^{17}O$ signal in air is largely a problem of improperly defined reference frames. In this work we refer to a deficit in ^{17}O relative to what one would expect if there were no respiration β and source-water effects and if there were no MIF effects to be transferred to O_2. In other words, our "deficit" in ^{17}O relative to ^{16}O refers to the situation in which O_2 exists with no biological or MIF influences. As an illustration of this reference state, we show in Fig. 5 the model result for $\Delta'^{17}O$ O_2 in which $\beta_{resp} = \beta_{water} = 0.528$ and the mass-independent component of fractionation attending ozone formation is removed (by setting α_{MIF} to 1.000). In the absence of both effects, O_2 lies effectively on the water reference line (Fig. 5). The definition of the ^{17}O deficit is in keeping with the definition of the Dole effect as being an "excess" in ^{18}O relative to ^{16}O as compared to expectations in the absence of biological kinetic isotope fractionation effects. The water reference line with $\lambda = 0.528$ (using λ rather than β or β_{eff} to avoid connotations of the origin of the slope) defines a suitable reference frame because water is the ultimate source of atmospheric O_2 and $\lambda = 0.528$ characterizes most natural waters (Meijer and Li, 1998). Waters (setting aside the spatially localized phenomenon of transpiration) retain a single λ value because of the much greater atomic mass of O compared with that of its bond partner H (Young et al., 2002). Even for extensive fractionation by Rayleigh evaporation, the β_{eff} is essentially indistinguishable from the β that obtains for equilibrium isotope fractionation between water phases. The reader can verify the constancy of β for water by applying Eqs. (13) through (15) to water vapor–liquid separation by a Rayleigh process using the equilibrium α and β values. In addition, the water three-isotope slope λ is similar to high-temperature equilibrium β values that obtain in the absence of kinetic isotope effects.

Angert et al. (2003) remarked that earlier proposals by Young et al. (2002) that the "major origin" of the ^{17}O deficiency in the atmosphere is from respiration was flawed because of the choice to compare air to a reference line with a higher slope than air itself. We emphasize that the prediction

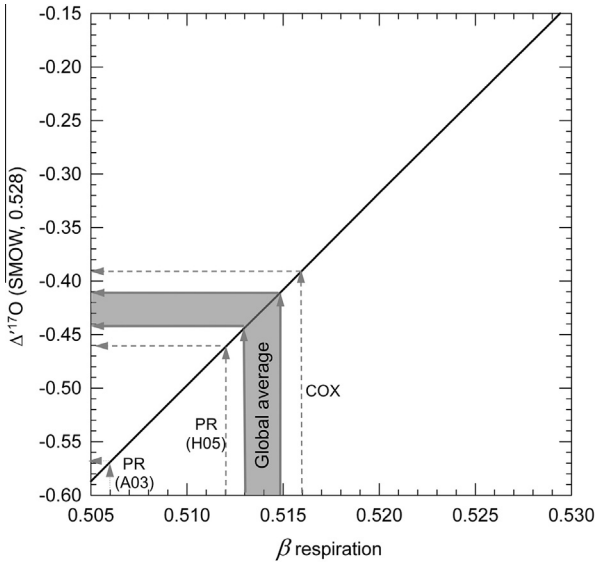

Fig. 6. Plot showing the effect of the respiration β value, β_{resp}, on $\Delta'^{17}O$ O_2 relative to the water reference line in three-isotope space (water line defined by $\lambda = 0.528$) obtained by numerical solutions to the box model. The range in global average values is defined by weighted summations of an upper bound on β values corresponding to the cytochrome pathway (COX, Angert et al., 2003) and a lower bound defined by photorespiration (PR, Angert et al., 2003, AO3, or Helman et al., 2005, H05). All $\Delta'^{17}O$ values correspond to the single model $\delta'^{18}O$ for O_2 (23.2‰).

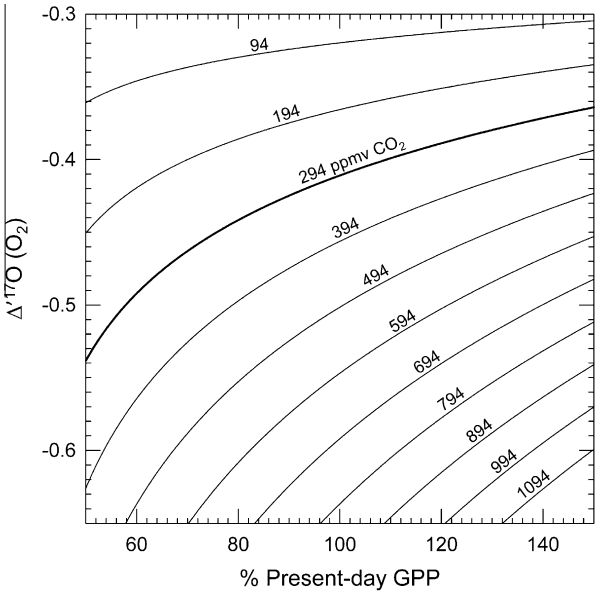

Fig. 7. Calculated effects of both gross primary production relative to present-day values, % GPP, and $[CO_2]$ on $\Delta'^{17}O$ O_2. Each contour represents the variation in $\Delta'^{17}O$ O_2 with% GPP at the fixed CO_2 concentration indicated by the label. Net primary production, and therefore $[O_2]$, is constant at present-day values in this diagram.

of the present model is precisely that the major component (nearly 2/3) of the ^{17}O deficiency is indeed respiration as deduced using an absolute reference frame defined by oxygen isotope ratios: with no respiration β effect, the $^{17}O/^{16}O$ of O_2 at the same $^{18}O/^{16}O$ would be 0.235‰ higher than the measured value, while with no stratosphere contribution, $^{17}O/^{16}O$ of O_2 at the same $^{18}O/^{16}O$ would be higher by 0.134‰ than the measured value. This result is a prediction that can be tested by comparing oxygen isotope ratio measurements of air, water, and rock (e.g., Fig. 1). This test is in no way nullified by the lack of oxygen isotope exchange between air and rock on 10^3 to 10^4 year timescales. Neither is it nullified by ignoring the fact that the β values for respiration are lower than the values that apply to rocks and waters.

4.3. Factors controlling $\Delta'^{17}O$ of O_2 and applications

The precise value for $\Delta'^{17}O$ O_2 depends on the β for respiration all else equal. Fig. 6 shows the range in estimates for β_{resp} and the effect on the present-day $\Delta'^{17}O$ O_2 using the model in this study. The range in global average β_{resp} values (shaded region in Fig. 6) reflects the ranges in values for photorespiration reported in the literature. Fig. 6 illustrates that uncertainties in, or changes in, β_{resp} in the third decimal digit translate into uncertainties or changes in $\Delta'^{17}O$ O_2 of 0.02‰ (20 per meg), all else equal. It is clear that alterations in the relative contributions of the different respiration pathways on a global scale could influence $\Delta'^{17}O$ O_2 in principle. In practice this effect may be small. Using the fractions of total respiration attributable to photorespiration today and in the last glacial episode cited by Blunier et al. (2002), the calculated shift in the global β_{resp} is 0.0002, corresponding to shifts in $\Delta'^{17}O$ O_2 at single digit per meg levels.

The ^{17}O deficit in atmospheric O_2 also depends on the rate of O_2 turnover by GPP, the concentration of O_2 determined by NPP, and the concentration of CO_2 in the atmosphere. We can treat GPP and $[CO_2]$ as independent variables in our model to arrive at the contour diagram shown in Fig. 7. The diagram shows the steady-state $\Delta'^{17}O$ O_2 values as a function of GPP and $[CO_2]$. In order to construct the diagram we varied GPP at fixed $[CO_2]$ by altering k_r and r_p, while holding net primary production, r_p/k_r, and therefore $[O_2]$, constant. Then we fixed GPP but varied the balance between volcanic delivery of CO_2 and uptake of CO_2 by weathering to produce various steady-state values for $[CO_2]$. The isopleths for $[CO_2]$ in Fig. 7 are precise fits to multiple numerical solutions at fixed CO_2 concentration. The equation for the 294 ppmv isopleth in Fig. 7 is $\Delta^{17}O = -0.7397 + 0.07941\ \ln(|37.3110 - \%GPP|)$. The result illustrates that both GPP and $[CO_2]$ are critically important to $\Delta'^{17}O$ O_2 and that the relationships are not strictly linear. For example, a change in $\Delta'^{17}O$ O_2 of approximately −50 per meg relative to the present day could result from an increase in CO_2 of 100 ppmv or a decrease in GPP to 70% of present-day values, or some combination thereof. A decrease in GPP to 70% of today's value with $[CO_2] = 494$ ppmv would correspond to a shift in $\Delta^{17}O$ O_2 of −80 per meg rather than −50 per meg predicted for pre-industrial $[CO_2]$.

As a real-world example, consider the last glacial maximum (LGM) examined by Blunier et al. (2002). They found air trapped in glacial ice with $\Delta^{17}O$ more positive than today by ~0.04‰. With $[CO_2]$ of ~190 ppmv during the LGM (Smith et al., 1997; Monnin et al., 2001) the expected shift in $\Delta'^{17}O$ O_2 with no changes in GPP is +0.04‰. In the absence of any additional evidence to the contrary, the observed change in $\Delta'^{17}O$ can be attributed solely to the reduced concentration of CO_2 during the LGM. Adding to this the effects of 80% GPP relative to present-day would suggest $\Delta'^{17}O$ O_2 values more positive than today by 0.055‰ based on our model.

Previous studies have sought to constrain $[CO_2]$ in deep time with $\Delta^{17}O$ values. Bao et al. (2008) found $\Delta^{17}O$ as low as −0.7‰ in sulfates in cap carbonates deposited as the Neoproterozoic global glaciation came to a close. Based on ~10% of the oxygen in marine sulfate coming from atmospheric O_2, Bao et al. estimated that the $\Delta^{17}O$ O_2 at that time was ~ −7‰ and that this markedly negative $\Delta^{17}O$ O_2 was the consequence of ~12,000 ppmv CO_2. We can use our model to assess these data. Fig. 8 shows our steady-state results for extreme enrichments in CO_2 relative to today for 100% and for 50% of present-day GPP. The model suggests that the inferred $\Delta^{17}O$ O_2 for the Neoproterozoic cap-carbonate time could have been the consequence of 20,000 ppmv for 100% of present GPP. The predicted $[CO_2]$ drops to ca. 10,000 ppmv for 50% GPP. By extrapolation, a very low level of GPP could reduce the $[CO_2]$ to ca. 1000 ppmv or less. Sansjofre et al. (2011) and Cao and Bao (2013) focused on the influence of NPP (i.e., $[O_2]$) in their assessments of the significance of the highly negative $\Delta^{17}O$ values in Neoproterozoic sulfates. In our calculations, the effect of decreasing r_p by half, and thus $[O_2]$ by half, is to decrease the steady-state $\Delta'^{17}O$ O_2 from −0.410‰ to −0.539‰, as discussed below.

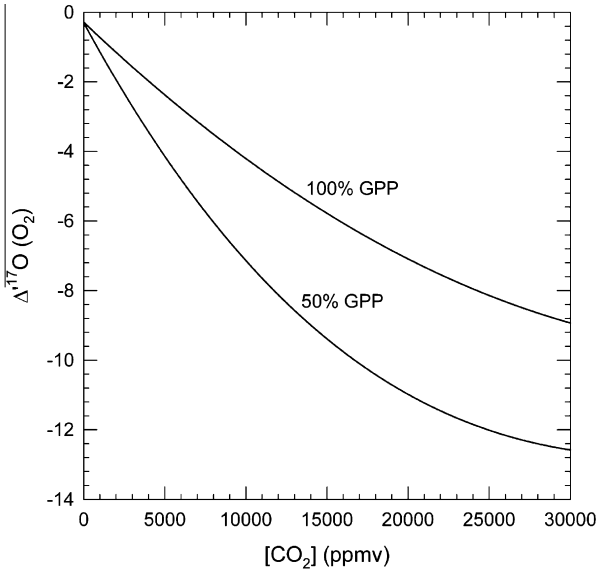

Fig. 8. Model results showing the effect of extreme CO_2 concentrations on $\Delta'^{17}O$ O_2 for two different levels of GPP relative to today (% GPP).

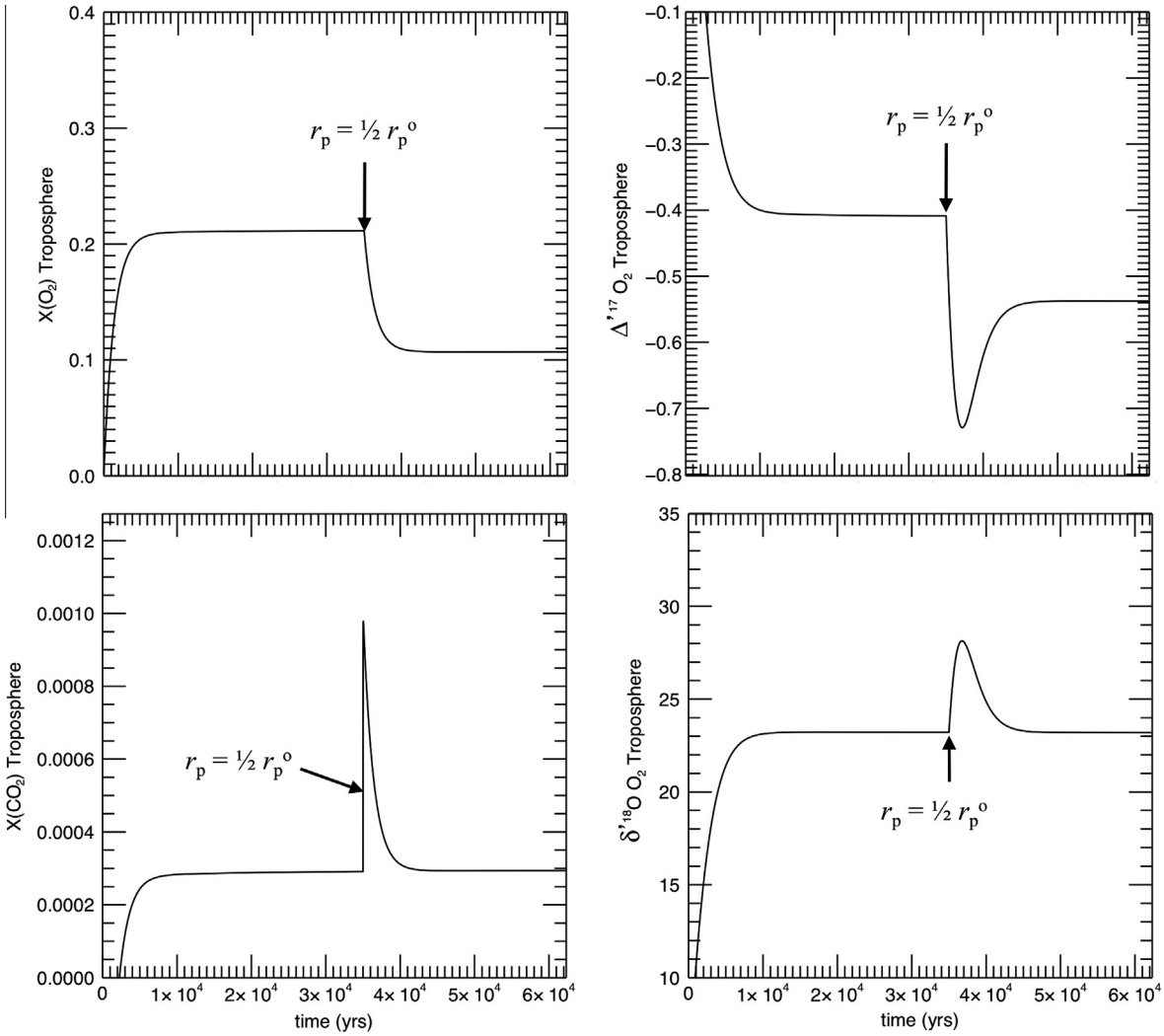

Fig. 9. Calculated effects of a sudden drop in the rate of photosynthesis by ½ at fixed respiration rate (thereby altering NPP). $X(O_2)$, upper left, is the mixing ratio of O_2. An initial spike in CO_2 concentration (lower left, $X(CO_2)$) drives a transient in both $\Delta'^{17}O$ (upper right) and $\delta'^{18}O$ in O_2 (lower right).

4.4. Time dependence

Time-dependent responses to shifts in factors controlling $\Delta'^{17}O$ O_2 are illustrated for two cases here, one triggered by a change in net primary production and the other initiated by a change in CO_2 concentration. In both cases we apply an instantaneous change to illustrate the response behavior.

Fig. 9 shows the result of a model with an initial condition of no O_2 and nominal rate coefficients (Table 2). After reaching steady state (Table 3) a reduction in the rate of photosynthesis to half the nominal value was introduced instantaneously. The result of this sudden shift in NPP is a transient negative $\Delta'^{17}O$ O_2 that lasts for another ~10,000 years until a new steady state is attained with a lower $\Delta^{17}O$ value (shift from −0.410‰ to −0.539‰, Fig. 9). The transient in $\Delta'^{17}O$ is triggered by a spike in $[CO_2]$ and a monotonic decline in $[O_2]$ incurred by the sudden reduction in photosynthesis (Fig. 9). This $[CO_2]$ spike lasts ~5000 years. The reduction in r_p also triggers a transient in $\delta'^{18}O$ O_2. The shift from 23.2‰ to 28.0‰ at the peak of the transient (Fig. 9) is the result of the decline in O_2 production, allowing respiration to exert greater influence on the isotopic composition of O_2. The positive-$\delta'^{18}O$ pulse contributes 0.06‰ to the negative $\Delta'^{17}O$ O_2 signal at the peak of the transient (i.e., (28.0–23.2) (0.5280–0.5149) = 0.063), a small fraction of the total shift. While $\Delta'^{17}O$ O_2 is altered permanently, the $\delta'^{18}O$ O_2 returns to the initial steady-state value of 23.2‰ after the 10^4 year transition. The existence of transient behaviors such as those shown in Fig. 9 could influence the interpretation of variations in $\Delta'^{17}O$ O_2 over 10^4 year timescales.

The second example of time-dependent behavior is addition of a pulse of CO_2 in which $[CO_2]$ increases instantaneously from 294 ppmv to 400 ppmv. It is meant as a crude simulation of the shift from pre-industrial CO_2 to present-day CO_2 concentrations over the relatively short time interval of ~150 years. The instantaneous pulse in $[CO_2]$ triggers a gradual decline in $\Delta'^{17}O$ O_2 that persists for ~4 *e*-fold residence times of O_2 (Fig. 10). The conclu-

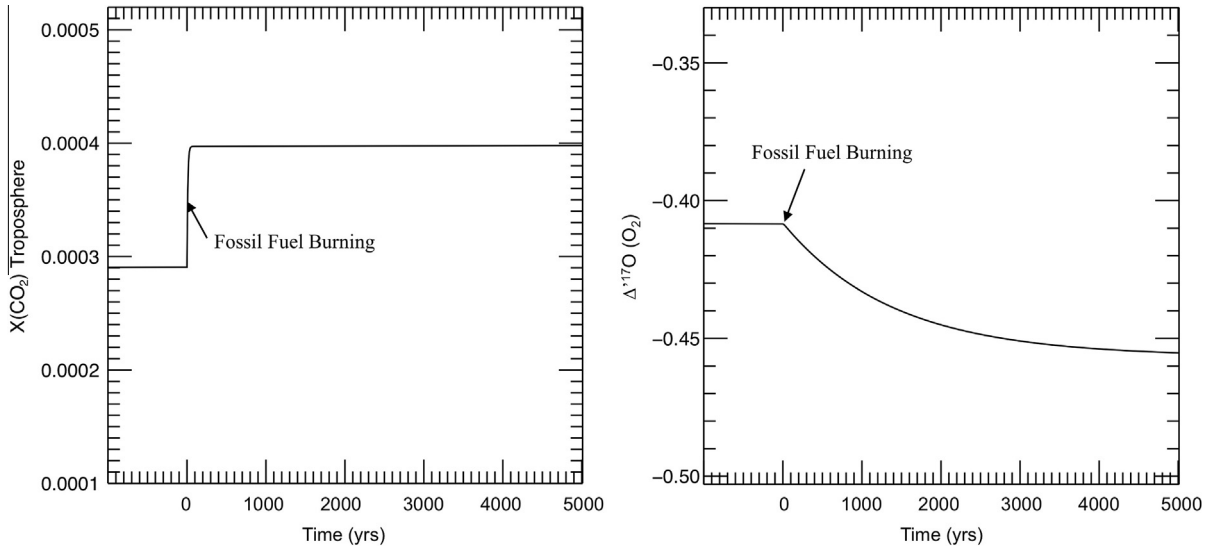

Fig. 10. The calculated effects of an instantaneous addition of tropospheric CO_2. The relatively slow response time of 4–5 residence times of O_2 (4–5 kyear) compared with 200 years of the industrial revolution means that the effects of industrial-revolution increases in $[CO_2]$ are not yet manifest in $\Delta'^{17}O$ O_2 beyond the single digit per-meg level.

sion is that the recent rise in atmospheric $[CO_2]$ has influenced the present-day $\Delta'^{17}O$ O_2 by $\leqslant 10$ per meg.

5. TESTS OF THE PREDICTED $\Delta'^{17}O$ O_2

Until very recently it has been assumed that rocks define an oxygen three-isotope trend that passes through the origin on a plot of $\delta'^{17}O$ vs. $\delta'^{18}O$ relative to SMOW (VSMOW in practice). This trend is characterized by a slope λ that is very nearly the same as high-temperature β values with most lines defined by λ between 0.525 and 0.528 (Meijer and Li, 1998; Rumble et al., 2007; Tanaka and Nakamura, 2012). Waters also define a line through the SMOW origin in logarithmic three-isotope space with a slope of $0.528 \pm \sim 0.001$ (Meijer and Li, 1998; Barkan and Luz, 2005). In essence, Earth's rocks and waters appear to define a "terrestrial fractionation line" that consists of tightly clustered lines with slopes λ of between 0.525 and 0.528 and a common intercept (we will come back to the latter assumption below). These lines comprising the "terrestrial fractionation line" (in quotations because it is not a single line in fact) have slopes similar to those predicted for equilibrium isotope fractionation. Atmospheric O_2 lies below this cluster of lines in three-isotope space (Fig. 1). We have characterized the ^{17}O deficit in air O_2 with respect to one version of this line with $\lambda = 0.528$ in our model calculations (corresponding to that for waters). For comparison, the predicted $\Delta'^{17}O$ O_2 of $-0.410‰$ relative to waters (and to terrestrial lines in general) can be tested by direct comparisons between the oxygen isotopic compositions of SMOW, atmospheric O_2, and rocks. Relatively few such comparisons exist.

5.1. Air O_2 isotopic measurements

We have measured the $^{17}O/^{16}O$ and $^{18}O/^{16}O$ ratios of atmospheric O_2 for the past three years. Our measurements are made relative to a reference gas that has been calibrated using the isotopic composition of San Carlos olivine using infrared laser-heating assisted fluorination. In addition, we obtain $\delta^{18}O$ values for meteorites that are comparable to those obtained at the University Chicago using this reference gas. The Chicago laboratory was originally calibrated by fluorinating SMOW. The $^{18}O/^{16}O$ of San Carlos olivine relative to SMOW is well known (e.g., 5.28 ± 0.10 $(1\sigma)‰$, Kusakabe and Matsuhisa, 2008). Like SMOW itself, the $^{17}O/^{16}O$ is less well known. We calibrated the reference tank O_2 under the assumption that $\Delta'^{17}O$ as defined by Eq. (5) is zero for San Carlos olivine. This nor-

Table 4
Typical rock three-isotope data taken relative to the reference tank used to measure Air O_2 at UCLA. All values are on the VSMOW scale.

	$\delta^{17}O$	st.dev.	1s.e.	$\delta^{18}O$	st.dev.	1s.e.	$\Delta^{17}O$[d] (0.528)	st.dev.	1s.e.	$\Delta^{17}O$[d] (0.527)	st.dev.	1s.e.
San Carlos olivine[a]	2.726	0.060	0.012	5.177	0.113	0.023	−0.004	0.028	0.006	−0.001	0.028	0.006
Gore Mtn. Garnet[b]	2.972	0.028	0.007	5.678	0.060	0.015	−0.021	0.024	0.006	−0.018	0.007	0.002
Oliver Quary Qtz[c]	5.436	0.016	0.008	10.359	0.019	0.010	−0.021	0.009	0.004	−0.013	0.013	0.007

[a] Reported value relative to VSMOW directly is $\delta^{18}O = 5.3 \pm 0.1‰$ (Tanaka and Nakamura, 2012; Kusakabe and Matsuhisa, 2008).
[b] Typical reported values are $\delta^{18}O = 5.7 \pm 0.1‰$.
[c] Typical reported values are $\delta^{18}O = 10.0 \pm 0.2‰$.
[d] Calculated using Eq. (5) and $\delta' = 10^3 \ln(\delta/10^3 + 1)$ values. 0.527 is our regressed slope for these samples (see text).

Table 5
Oxygen isotopic ratios of air O_2 measured at UCLA. All values relative to VSMOW.

Date	$\delta^{17}O$	$\delta^{18}O$	$\delta'^{17}O$	$\delta'^{18}O$	$\Delta^{17}O$ (0.528, per meg)
9/21/11	11.974	23.520	11.903	23.248	−371.5
9/22/11	11.991	23.562	11.920	23.289	−376.2
9/22/11	11.990	23.554	11.919	23.281	−373.5
9/23/11	11.990	23.569	11.919	23.295	−381.3
9/27/11	11.997	23.575	11.925	23.302	−377.9
10/19/11	11.923	23.447	11.852	23.176	−384.8
10/21/11	11.969	23.525	11.898	23.253	−379.2
7/26/12	11.958	23.494	11.888	23.222	−373.6
8/8/12	12.002	23.576	11.931	23.302	−372.9
8/17/12	11.967	23.503	11.896	23.231	−369.8
8/22/12	11.980	23.527	11.909	23.255	−369.6
8/27/12	11.952	23.457	11.881	23.186	−361.2
2/28/13	11.916	23.417	11.846	23.148	−376.2
3/18/13	11.946	23.476	11.875	23.204	−376.5
3/20/13	12.000	23.570	11.929	23.297	−372.1
3/30/13	12.002	23.588	11.930	23.314	−379.9
5/7/13	11.991	23.552	11.920	23.279	−371.2
5/8/13	12.011	23.596	11.940	23.322	−374.1
5/9/13	12.009	23.587	11.938	23.313	−371.5
5/20/13	11.965	23.516	11.894	23.244	−378.3
5/21/13	11.985	23.552	11.914	23.278	−377.4
6/1/13	12.002	23.588	11.930	23.314	−379.7
6/3/13	11.972	23.527	11.901	23.255	−377.9
6/18/13	12.009	23.589	11.938	23.316	−373.1
6/19/13	12.002	23.578	11.931	23.304	−373.7
6/24/13	11.986	23.548	11.914	23.275	−374.7
6/25/13	11.973	23.512	11.902	23.240	−368.6
6/26/13	11.980	23.520	11.909	23.248	−366.2
6/28/13	11.956	23.475	11.885	23.204	−366.8
7/1/13	11.982	23.536	11.910	23.263	−372.3
7/2/13	11.976	23.518	11.905	23.246	−369.0
7/6/13	11.988	23.541	11.917	23.268	−368.8
7/8/13	11.985	23.537	11.914	23.264	−369.6
7/14/13	11.998	23.560	11.927	23.286	−368.4
7/21/13	11.977	23.531	11.906	23.259	−374.3
7/28/13	11.981	23.540	11.910	23.267	−375.3
8/7/13	11.931	23.447	11.860	23.176	−377.0
Average	11.979	23.533	11.908	23.260	−373.6
Std. Dev.	0.023	0.045	0.023	0.044	4.8

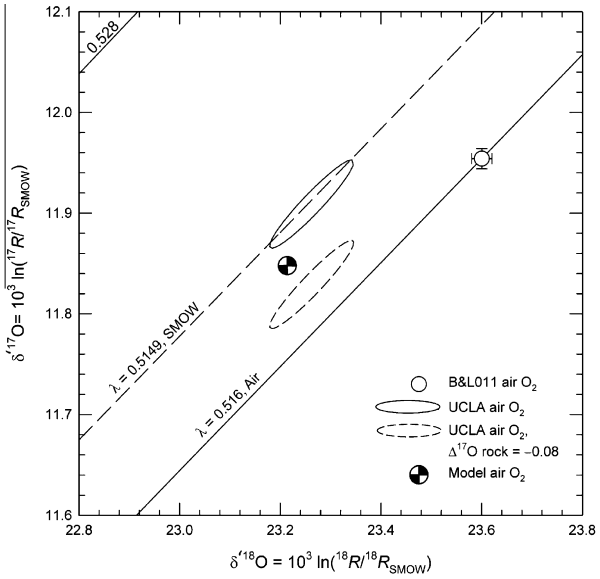

Fig. 11. Three-isotope plot (relative to SMOW) comparing the air O_2 isotope ratios obtained in this study (solid 2σ error ellipse) with the model air O_2 (black and white circle). Also shown are the UCLA air O_2 composition corrected for the possible offset in $\Delta^{17}O$ between water and San Carlos olivine (see text), shown as the dashed error ellipse, and the air O_2 composition relative to VSMOW obtained by Barkan and Luz (2011, B&L011) shown as the open circle. Also shown for reference are the water fractionation line with $\beta = \lambda = 0.528$ (upper solid line) passing through the origin, the model respiration fractionation line for air O_2 ($\beta = \lambda = 0.5149$, dashed) passing through the origin, and the respiration line of B&L011 ($\beta = \lambda = 0.516$) forced through their measured air value and not the origin.

malization gives the correct $\Delta'^{17}O$ values among different meteorite groups in our laboratory where inter-laboratory comparisons are available to at least the 0.02‰ level of precision. However, because fractionation slopes in three-isotope space for rocks vary, and because it is not generally possible to define $\delta'^{17}O$ (SMOW) on the basis of a single rock datum, there is an inherent accuracy uncertainty in the above procedure amounting to ~5.2 (0.528–0.525) = 0.016‰ (16 per meg). Recent data for three recognized reference rock materials obtained with our laser fluorination system are shown in Table 4, establishing the accuracy of the $\delta^{18}O$ values. The data were obtained using analytical methods essentially the same as those described by Young et al. (1998a,b). Because we work at a precision of 0.02‰ or better for meteorite studies, we pay particular attention to removing NF_3 cryogenically on molecular sieves, ensuring that there are no $m/z = 33$ interferences from NF^+. These data define a λ of 0.527 ± 0.002 (1σ) and an intercept of 0.002 (York regression, Mahon, 1996).

Some of our results for air have been discussed previously (Yeung et al., 2012a,b) and our methods used to collect the data shown in Table 5 follow the same procedures. In brief, we analyze $^{17}O/^{16}O$ and $^{18}O/^{16}O$ in O_2 following removal of N_2 and Ar by gas chromatography (GC) at sub-ambient temperatures (<−65 °C). The GC is attached to a vacuum extraction line. Following expansion into the vacuum system, air samples are adsorbed onto degassed silica gel in a cryogenic stainless steel U-trap at −196 °C for ~30 min. The gas is then eluted at ~60 °C under flowing high-purity helium. The analyte is injected into a 3-m molecular sieve 5A GC column using a He-purged 4-way switching valve at a flow rate of 25 mL min^{-1}. The eluent from the GC column is collected on a second silica gel U-trap at −196 °C. Most samples are passed through the GC system twice. Baseline separation of Ar, O_2, and N_2 is achieved at our run conditions; Ar–O_2 separation times are 8 min with O_2 peak full widths of ~20 min. With two passes through the GC column air samples contain <5 ppm Ar. At this level of purity, correction for ion scat-

tering is not necessary. We have also analyzed air samples with cryogenic separation of N_2 and O_2 on molecular sieve but with no GC separation, requiring correction for the presence of Ar. Our results with that method are similar to those reported here based on GC purification.

Molecular oxygen isotope ratio measurements are made on a ThermoFinnigan MAT 253 gas-source isotope ratio mass spectrometer (irms). Oxygen extracted from rock is normally analyzed on a ThermoFinnigan Delta irms instrument. We measured O_2 from both sources on both mass spectrometers (using the dual inlets in both cases) to ensure no instrument-specific bias. None was found.

The mean composition of 37 analyses of air from 9/21/11 to 8/7/13 is $\delta^{17}O = 11.979 \pm 0.023$ (1σ), $\delta^{18}O = 23.533 \pm 0.045$ (1σ) and $\Delta'^{17}O$ (Eq. (5), $\beta = \lambda = 0.528$, zero intercept) $= -0.373 \pm 0.005$‰ (1σ). The logarithmic values are $\delta'^{17}O = 11.908$ and $\delta'^{18}O = 23.260$‰. Fig. 11 compares our air data with the model predicted value in three-isotope space. The air data are displayed as a 2σ error ellipse calculated from the eigenvalues and eigenvectors of the 2-D covariance matrix for $\delta'^{17}O$ and $\delta'^{18}O$. The difference of 0.037‰ between the measured air $\Delta^{17}O$ O_2 and the model predicted value (−0.373‰ vs. −0.410‰) at face value would seem to invalidate the predicted value. However, our measurement assumes that San Carlos olivine has $\Delta'^{17}O = 0.0$ to an accuracy uncertainty of ~20 per meg. The validity of this assumption has been thrown into question by recent analyses comparing rocks to SMOW directly. These findings are discussed in the next section.

5.2. Comparing rock and SMOW $\Delta'^{17}O$

Tanaka and Nakamura (2012) measured the oxygen isotopic composition of natural silicate and oxide minerals directly against that of VSMOW using irms. They find that twenty analyses of San Carlos olivine yield a $\Delta'^{17}O$ of -0.076 ± 0.021 (1σ)‰ on the VSMOW scale where $\Delta'^{17}O$ is calculated as in Eq. (5) with their rock slope of 0.5270 ± 0.0005. These measurements were verified by Pack and Herwartz (2014) and apparently invalidate the assumption of $\Delta'^{17}O = 0$ for rocks at $\delta^{18}O = 0$ relative to SMOW. We note that Kusakabe and Matsuhisa (2008) also compared rocks with SMOW and SLAP directly and based on regressions of their water and rock data there appears to be no clear offset in the intercepts in three-isotope space. Nonetheless, in order to correct for the observations of Tanaka and Nakamura (2012) and Pack and Herwartz (2014), we adjusted our standard to accommodate a −0.08‰ $\Delta^{17}O$ for San Carlos olivine (correction $= -0.08 + 5.2(0.528–0.527)$, the latter term being an estimate for the effect of slope alone in our laboratory) relative to the water reference line. The adjusted values for our air analyses are $\delta^{17}O = 11.898 \pm 0.023$ (1σ), $\delta'^{17}O = 11.828 \pm 0.023$ (1σ), and $\Delta^{17}O = -0.454 \pm 0.005$ (1σ)‰ ($^{18}O/^{16}O$ values are unaffected). Our adjusted measurements are more negative in $\Delta'^{17}O$ than the predicted value by 0.044‰. The position of the air datum corrected for the offset is shown as a 2σ error ellipse in Fig. 11.

In summary, measured air O_2 triple oxygen isotope ratios determined by comparisons with rocks straddle the predicted air O_2 $\Delta'^{17}O$ value depending upon the intercept of rock data relative to SMOW (i.e., $\Delta'^{17}O$ of rocks as measured at $\delta^{18}O = 0.0$‰ relative to SMOW). In order for our measured values for air to agree with the predicted value, the $\Delta^{17}O$ intercept of rock fractionation lines relative to SMOW would have to be ~ −0.04 rather than the −0.08‰ suggested by recent measurements.

5.3. Comparisons with previous work

Pack et al. (2007) used an approach similar to that described above to arrive at an air O_2 $\Delta'^{17}O$ value of -0.344 ± 0.015 (1s)‰, similar to the value we obtain. This measurement, like ours, relies on a zero intercept of the rock fractionation line (or family of lines) on the SMOW scale in three-isotope space. Adjusting the Pack et al. (2007) value for the offset between SMOW and mantle olivine suggests an air $\Delta^{17}O$ of −0.422, within error of the predicted value.

Direct comparisons between air O_2 and VSMOW bypass the intermediate step of comparing rocks to VSMOW and then comparing O_2 to rocks. There is, to our knowledge, one set of measurements of atmospheric O_2 relative to VSMOW in the era of modern instrumentation with per meg level precision and this is by Barkan and Luz (2005) and later Barkan and Luz (2011) (hereafter B&L11). Recasting the more recent results of B&L11 in terms of atmospheric O_2 relative to VSMOW, the values are $\delta^{17}O = 12.026 \pm 0.01$ (95%), $\delta^{18}O = 23.881 \pm 0.02$ (95%) and $\Delta'^{17}O$ (Eq. (5), $\beta = \lambda = 0.528$, zero intercept) $= -0.506 \pm 0.004$‰ (95%). The corresponding logarithmic values are $\delta'^{17}O = 11.954$ and $\delta'^{18}O = 23.600$‰. These values are shown for comparison in Fig. 11. The disparity between the model prediction for air O_2 $\Delta'^{17}O$ and the B&L11 air measurements is nearly 0.1‰. Our adjusted air measurements are essentially midway between our unadjusted measurements and the B&L11 value. We note that the older $\Delta'^{17}O$ values for air O_2 relative to VSMOW of Barkan and Luz (2005) and our adjusted $\Delta'^{17}O$ agree (-0.454 ± 0.01 (2σ) and -0.453 ± 0.01 (95%)‰, respectively). Kaiser (2008) renormalized prior $\delta^{17}O$ and $\delta^{18}O$ values vs VSMOW arriving at values of 12.32‰ and 24.36‰, respectively, corresponding to $\delta'^{17}O = 12.24$, $\delta'^{18}O = 24.06$‰, and $\Delta'^{17}O = -0.463$. The latter is within error of our adjusted measurements and 0.05‰ more negative than the prediction.

Agreement is not achieved between the predicted value and the most recent direct SMOW-air O_2 comparisons. The sensitivity of the calculated air O_2 $\Delta'^{17}O$ values to the model input parameters is discussed in the following section.

6. MODEL SENSITIVITY

The closure error for the $\Delta'^{17}O$ budget as depicted in our model is between 0‰ and ~0.1‰. The larger value is significant and would imply a commensurately significant error in model input parameters. We have already described variations in predicted $\Delta'^{17}O$ of O_2 values with variations in [CO_2], GPP and NPP. Here we consider the possibility that

there are significant errors in the various rate coefficients and fluxes in Table 2.

The calculated $\Delta'^{17}O$ of atmospheric O_2 is directly proportional to β_{water} for the globally-averaged water sources. A $\Delta'^{17}O$ of atmospheric O_2 of -0.506 (B&L11) can be matched by the calculations if β_{water} is 0.502, all else equal. The $\Delta'^{17}O$ of atmospheric O_2 values of ~ -0.45 obtained by comparisons with rocks after correction for non-zero intercepts on the SMOW scale are accommodated if β_{water} is 0.512 (close to expectations from fractionation by diffusion or evaporation of molecular water). Existing measurements for transpiration, however, are between 0.522 and 0.514 depending upon humidity (Landais et al., 2006). At face value the mismatches between the lowest measured air O_2 $\Delta'^{17}O$ values and the predicted value are not accommodated by β_{water} alone. However, if the absolute value of the intercept of rock $\Delta'^{17}O$ relative to SMOW is more positive than $-0.08‰$, the gap between measured $\Delta'^{17}O$ O_2 obtained by comparisons with rocks and calculated values can be closed.

The model result is relatively robust with respect to stratosphere–troposphere mixing. For example, increasing this mixing rate by 10-fold changes the predicted $\Delta'^{17}O$ of O_2 by just $-0.05‰$ (i.e., the value becomes more negative). The reason is that the rate of stratosphere-troposphere mixing alters the $\Delta'^{17}O$ CO_2 flux and $\Delta'^{17}O$ of stratospheric CO_2 in opposite directions, forming a feedback that in essence protects O_2 from large variations in $\Delta'^{17}O$. However, increasing the transport rate by a factor of 10 causes the bulk stratospheric $\Delta'^{17}O$ of CO_2 to decline from 1.6‰ to 0.3‰, a value that appears to be much too low. If we take the B&L11 air O_2/SMOW measurements at face value, adjustments in mixing cannot solve the apparent mass balance closure error.

Although our stratosphere chemistry reaction network yields reasonable $[O_3]$ and $\Delta'^{17}O$ CO_2 values, and the troposphere rates are well constrained, it is instructive to consider the effects of varying the reaction rate constants about their nominal values. Increasing the CO_2–H_2O oxygen isotope exchange rate by 10-fold has virtually no effect on $\Delta'^{17}O$ O_2; the adjustments occur in $\Delta'^{17}O$ of CO_2 instead. Increasing the rate of stratospheric O_2 photolysis by an order of magnitude decreases $\Delta'^{17}O$ O_2 from $-0.41‰$ to $-0.64‰$. This decrease is driven by an increase in $\Delta'^{17}O$ CO_2 flux to $24 \times 10^{15}‰$ moles year^{-1}, a value nearly 10× greater than the measured value (although our nominal model value is already high by a factor of 2–3). Similarly, increasing the rate of O_3 photolysis by 10-fold also raises the $\Delta'^{17}O$ CO_2 flux to $24 \times 10^{15}‰$ moles year^{-1} with the same effect on $\Delta'^{17}O$ O_2. An actinic flux greater than that used in Table 2 might be warranted in that ozone is mainly produced at equatorial latitudes. This would result in an increase in both O_2 and O_3 photolysis rates. Increasing *both* photolysis rates by 10-fold leads to no change in the steady state $[O_3]$ (due to cancellation of the two rates that are a source and a sink for O_3, respectively) but reduces $\Delta'^{17}O$ O_2 to $-1.1‰$; a factor of 10 in photolysis rates triples the magnitude of the $\Delta^{17}O$ O_2 (because the stratosphere influence on $\Delta^{17}O$ O_2 is $\sim$1/3). We note that the increase in actinic fluxes from ca. 30° solar zenith to 0° is a factor of order 1.1 to 1.2 rather than 10, so uncertainties in the flux are unlikely to be responsible for a large error in the calculated $\Delta'^{17}O$ O_2. As an example, tables for actinic flux vs. solar zenith angle (Finlayson-Pitts and Pitts, 2000) indicate an increase of 1.15 (15%) for 0° vs. 30°. Running our basic model with a 15% increase in J values for O_2 and O_3 photolysis results in a 4% decrease in $\Delta'^{17}O$ O_2, from $-0.410‰$ to $-0.428‰$. This decrease is the result of a 13% increase in $\Delta'^{17}O$ CO_2 flux. The difference is 5 times smaller than the closure error in the $\Delta'^{17}O$ budget if the B&L11 measurements are used as the benchmark (Fig. 11). When one considers that solar flux varied tens of per cent over 10^8 to 10^9-year timescales (Claire et al., 2012), this could be relevant for some deep-time applications however.

With regard to reaction rates, $\Delta'^{17}O$ O_2 is most sensitive to the rate of $O(^1D)$ quenching. Increasing the rate of $O(^1D)$ quenching by O_2 and O_3 10-fold yields a $\Delta'^{17}O$ O_2 of $-1.12‰$ and a $\Delta'^{17}O$ CO_2 flux of $50 \times 10^{15}‰$ moles year^{-1}. Here again, the $\Delta'^{17}O$ CO_2 flux is more than 10 times the measured value.

In summary, errors in the rate constants for reactions in the stratosphere on the order of 5- to 10-fold could cause an underestimation of $\Delta'^{17}O$ O_2. However, we see no indication that these constants are in error by this magnitude. More importantly, in each case, the lowering of $\Delta'^{17}O$ O_2 comes at the cost of an even higher $\Delta'^{17}O$ CO_2 flux, making this value greater than the uncertainties in the observations will allow by approximately an order of magnitude.

The most uncertain aspect of our model is not to be found in the rate constants but in the MIF fractionation factor attending ozone formation (see Section 3.2). The isotopic composition of $O(^1D)$ is the ultimate driver for $\Delta'^{17}O$ O_2. Some studies predict that the integrated $\Delta'^{17}O$ of $O(^1D)$ could be as high as 80‰ (Lyons, 2001; Yeung et al., 2009), mainly due to the concentration of the MIF anomaly in the terminal oxygens of O_3, while in our models $\Delta'^{17}O$ $O(^1D)$ is 27‰. We explored this as a possible explanation for the mass balance closure error for $\Delta'^{17}O$ O_2 that results from comparing the direct air-VSMOW measurements of B&L11 with our model results. With all else equal, the $\Delta'^{17}O$ $O(^1D)$ in the model can be adjusted to fit the B&L11 target $\Delta'^{17}O$ O_2 of $-0.506‰$ by adjusting α_{MIF}. We find that a $\Delta'^{17}O$ $O(^1D)$ value of 45.9‰ (resulting from $\alpha_{MIF} = 1.109$) reproduces the B&L11 value. It also lowers the model $\delta'^{17}O$ and $\delta'^{18}O$ values slightly to 11.65‰ and 23.01‰. The attending $\Delta'^{17}O$ CO_2 flux is $15 \times 10^{15}‰$ moles year^{-1} and the stratospheric $\Delta'^{17}O$ CO_2 is 2.8‰; as in all cases, lowering the $\Delta'^{17}O$ O_2 comes at the expense of further increasing the $\Delta'^{17}O$ CO_2 flux, in this case to a factor of $\sim$4 greater than the measured value. Our basic-model CO_2 isotopic flux is already high by a factor of 2–3 and a further increase to a factor of 4 or more would seem to push the boundaries of credibility.

7. CONCLUSIONS

Modeling the present-day $\Delta'^{17}O$ of atmospheric O_2 shows that 57% of the deficit in ^{17}O in O_2 relative to waters is the result of kinetic isotope fractionation attending the

Dole effect, 33% derives from the $\Delta'^{17}O$ of $O(^1D)$ in the stratosphere, and 10% is from evapotranspiration. The value for $\Delta'^{17}O$ O_2 varies in our calculations, in some cases non-linearly, with $[CO_2]$, gross primary production, and net primary production. Separating the influence of these three factors on measured $\Delta'^{17}O$ for extant samples of ancient O_2 or molecular oxygen proxies will require additional information. The sensitivity to changes in the proportions of respiration pathways is minor.

Our model prediction is consistent with measurements of air O_2 if rocks define fractionation lines with non-zero intercepts in $\delta'^{17}O$ vs. $\delta'^{18}O$ relative to SMOW of $\sim -0.04‰$, or about half that indicated by recent measurements. However, if rocks have intercepts of $\sim -0.07‰$ to $-0.08‰$ relative to SMOW, as recent measurements suggest, then the model $\Delta'^{17}O$ O_2 values are too positive by 0.04‰. If the correct $\Delta'^{17}O$ of O_2 relative to SMOW is $-0.51‰$ as another measurement indicates, then the model $\Delta'^{17}O$ O_2 is too positive by ~0.10‰. Such a large underestimate can only be ameliorated in our models by invoking an integrated (bulk) $\Delta'^{17}O$ for stratospheric CO_2 that is significantly greater than measurements currently allow.

Our results underscore the need for high-precision comparisons of the $^{17}O/^{16}O$ and $^{18}O/^{16}O$ ratios of atmospheric O_2, VSMOW, and rocks.

ACKNOWLEDGMENTS

The authors thank Prof. Edwin Schauble for conversations and advice on an earlier version of this work. We also thank James Farquhar and two anonymous reviewers for helpful critiques. Jeanine Ash is thanked for her help with air O_2 isotope ratio measurements and Karen Ziegler is thanked for her work on calibrating our reference gas using CO_2 laser fluorination of terrestrial and extraterrestrial rock samples.

REFERENCES

Angert A., Cappa C. D. and DePaolo D. J. (2004) Kinetic ^{17}O effects in the hydrologic cycle: indirect evidence and implications. *Geochim. Cosmochim. Acta* **68**, 3487–3495.

Angert A., Rachmilevitch S., Barkan E. and Luz B. (2003) Effects of photorespiration, the cytochrome pathway, and the alternative pathway on the triple isotopic composition of atmospheric O_2. *Global Biogeochem. Cycles* **17**, 1030.

Appenzeller C. and Holton J. R. (1996) Seasonal variation of mass transport across the tropopause. *J. Geophys. Res.* **101**(D10), 15071–15078.

Bao H., Lyons J. R. and Zhou C. (2008) Triple oxygen isotope evidence for elevated CO_2 levels after a Neoproterozoic glaciation. *Nature* **453**, 504–506.

Barkan E. and Luz B. (2005) High precision measurements of $^{17}O/^{16}O$ and $^{18}O/^{16}O$ ratios in H_2O. *Rapid Commun. Mass Spectrom.* **19**, 3737–3742.

Barkan E. and Luz B. (2011) The relationships among the three stable isotopes of oxygen in air, seawater and marine photosynthesis. *Rapid Commun. Mass Spectrom.* **25**, 2367–2369.

Beck W. C., Grossman E. L. and Morse J. W. (2005) Experimental studies of oxygen isotope fractionation in the carbonic acid system at 15, 25, and 40 °C. *Geochem. Cosmochim. Acta* **69**(14), 3493–3503.

Bender M. L., Sowers T. and Labeyrie L. (1994) The Dole effect and its variations during the last 130,000 years as measured in the Vostok ice core. *Global Biogeochem. Cycles* **8**, 363–376.

Biswas D. K., Xu H., Li Y. G., Ma B. L. and Jiang G. M. (2013) Modification of photosynthesis and growth responses to elevated CO_2 by ozone in two cultivars of winter wheat with different years of release. *J. Exp. Bot.* **64**, 1485–1496.

Blunier T., Barnett B., Bender M. L. and Hendricks M. B. (2002) Biological oxygen productivity during the last 60,000 years from triple oxygen isotope measurements. *Global Biogeochem. Cycles* **16**(3). http://dx.doi.org/10.1029/2001GB001460.

Boering K. A., Jackson T., Hoag K. J., Cole A. S., Perri M. J., Thiemens M. and Atlas E. (2004) Observations of the anomalous oxygen isotopic composition of carbon dioxide in the lower stratosphere and the flux of the anomaly to the troposphere. *Geophys. Res. Lett.* **31**, L03109, doi: 03110.01029/02003GL018451.

Cao X. and Bao H. (2013) Dynamic model constraints on oxygen-17 depletion in atmospheric O_2 after a snowball Earth. *Proc. Natl. Acad. Sci. USA*. http://dx.doi.org/10.1073/pnas.1302972110.

Cao X. and Liu Y. (2011) Equilibrium mass-dependent fractionation relationships for triple oxygen isotopes. *Geochem. Cosmochim. Acta* **75**, 7435–7445.

Claire M. W., Sheets J., Cohen M., Ribas I., Meadows V. S. and Catling D. C. (2012) The evolution of solar flux from 0.1 nm to 160 μm: quantitative estimates from planetary studies. *Astrophys. J.* **757**, 95, doi: 10.1088/0004-1637X/1757/1081/1095.

DeMore W. B., Sanders S. P., Golden D. M., Hampson R. F., Kurylo M. J., Howard C. J., Kolb C. E. and Molina M. J. (1997). Chemical Kinetics and Photochemical Data for Use in Stratospheric Modeling, Evaluation Number 12. Pasadena, CA, Jet Propulsion Laboratory.

Dole M. (1935) The relative atomic weight of oxygen in water and in air. *J. Am. Chem. Soc.* **57**, 2731.

Fabian P., Libby W. F. and Palmer C. E. (1968) Stratospheric residence time and interhemispheric mixing of strontium 90 from fallout in rain. *J. Geophys. Res.* **73**(12), 3611–3616.

Farquhar G. D., Lloyd J., Taylor J. A., Flanagan L. B., Syvertsen J. P., Hubick K. T., Wong S. C. and Ehleringer J. R. (1993) Vegetation effects on the isotope composition of oxygen in atmospheric CO_2. *Nature* **363**(3), 439–443.

Finlayson-Pitts B. J. and Pitts, Jr., J. N. (2000) *Chemistry of the Upper and Lower Atmosphere, Theory, Experiments, and Applications*. Academic Press, San Diego.

Francey R. J. and Tans P. P. (1987) Latitudinal variation in oxygen-18 of atmospheric CO_2. *Nature* **327**, 495–497.

Gao Y. Q. and Marcus R. A. (2002) On the theory of the strange and unconventional isotopic effects in ozone formation. *J. Chem. Phys.* **116**, 137–154.

Grewe V. (2005) The origin of ozone. *Atmos. Chem. Phys. Discus.* **5**, 9641–9668.

Guy R. D., Fogel M. L. and Berry J. A. (1993) Photosynthetic fractionation of the stable isotopes of oxygen and carbon. *Plant Physiol.* **101**, 37–47.

Hayes J. M. (2001) Fractionation of carbon and hydrogen isotopes in biosynthetic processes. In *Stable Isotope Geochemistry*, vol. 43 (eds. J. W. Valley and D. R. Cole). Mineralogical Society of America, Blacksburg, pp. 225–277.

Helman Y., Barkan E., Eistenstadt D., Luz B. and Kaplan A. (2005) Fractionation of the three stable oxygen isotopes by oxygen-producing and oxygen-consuming reactions in photosynthetic organisms. *Plant Physiol.* **138**, 2292–2298.

Hindmarsh A. C. (1983). ODEPACK, a systematized collection of ODE solvers. In *Scientific Computing* (eds. R. S. Stepleman and et al.). Amsterdam, North-Holland. pp. 55–64.

Hoffman G., Cuntz M., Weber C., Ciais P., Friedlingstein P., Heimann M., Jouzel J., Kaduk J., Maier-Reimer E., Seibt U. and Six K. (2004) A model of the Earth's Dole effect. *Global Biogeochem. Cycles* **18**(GB1008). http://dx.doi.org/10.1029/2003GB002059.

Holton J. R. (1990) On the global exchange of mass between the stratosphere and troposphere. *J. Atmos. Sci.* **47**, 392–395.

Hulston J. R. and Thode H. G. (1965) Variations in the S^{33}, S^{34}, and S^{36} contents of meteorites and their relation to chemical and nuclear effects. *J. Geophys. Res.* **70**, 3475–3484.

Jacobson M. Z. (2005) *Fundamentals of Atmospheric Modeling*. Cambridge University Press.

Janssen C. (2005) Intramolecular isotope distribution of heavy ozone ($^{16}O^{18}O^{16}O$ and $^{16}O^{16}O^{18}O$). *J. Geophys. Res.* **110**. http://dx.doi.org/10.1029/2004JD005479.

Janssen C., Guenther J., Krankowsky D. and Mauersberger K. (1999) Relative formation rates of $^{50}O_3$ and $^{52}O_3$ in ^{16}O–^{18}O mixtures. *J. Chem. Phys.* **111**(16), 7179–7182.

Janssen C., Guenther J., Krankowsky D. and Mauersberger K. (2003) Temperature dependence of ozone rate coefficients and isotopologue fractionation in ^{16}O–^{18}O oxygen mixtures. *Chem. Phys. Lett.* **367**, 34–38.

Kaiser J. (2008) Reformulated ^{17}O correction of mass spectrometric stable isotope measurements in carbon dioxide and a critical appraisal of historic 'absolute' carbon and oxygen isotope ratios. *Geochem. Cosmochim. Acta* **72**, 1312–1334.

Krankowsky D., Lammerzahl P., Mauersberger K., Janssen C., Tuzson B. and Rockmann T. (2007) Statospheric ozone isotope fractionations derived from collected samples. *J. Geophys. Res.* **112**. http://dx.doi.org/10.1029/2006JD007855.

Kroopnick P. and Craig H. (1972) Atmospheric oxygen: isotopic composition and solubility fractionation. *Science* **175**, 54–55.

Kump L. R., Brantley S. L. and Arthur M. A. (2000) Chemical weathering, atmospheric CO_2, and climate. *Ann. Rev. Earth Planet. Sci.* **28**, 611–667.

Kusakabe M. and Matsuhisa Y. (2008) Oxygen three-isotope ratios of silicate reference materials determined by direct comparison with VSMOW oxygen. *Geochem. J.* **42**, 309–317.

Landais A., Barkan E., Yakir D. and Luz B. (2006) The triple isotopic composition of oxygen in leaf water. *Geochem. Cosmochim. Acta* **70**, 4105–4115.

Lane G. and Dole M. (1956) Fractionation of oxygen isotopes during respiration. *Science* **123**, 574–576.

Lasaga A. C. and Ohmoto H. (2002) The oxygen geochemical cycle: dynamics and stability. *Geochim. Cosmochim. Acta* **66**, 361–381.

Liang M.-C., Blake G. A., Lewis B. R. and Yung Y. L. (2007) Oxygen isotopic composition of carbon dioxide in the middle atmosphere. *Proc. Natl. Acad. Sci. USA* **104**(1), 21–25.

Liang M.-C., Blake G. A. and Yung Y. L. (2008) Seasonal cycle of $C^{16}O^{16}O$, $C^{16}O^{17}O$, $C^{16}O^{18}O$ in the middle atmosphere: implications for mesospheric dynamics and biogeochemical sources and sinks of CO_2. *J. Geophys. Res.* **113**(D12305). http://dx.doi.org/10.1029/2007/JD008392.

Liang M.-C., Irion F. W., Weibel J. D., Miller C. E., Blake G. A. and Yung Y. L. (2006) Isotopic composition of stratospheric ozone. *J. Geophys. Res.* **111**. http://dx.doi.org/10.1029/2005JD006342.

Luz B. and Barkan E. (2005) The isotope ratios $^{17}O/^{16}O$ and $^{18}O/^{16}O$ in molecular oxygen and their significance in biogeochemistry. *Geochem. Cosmochim. Acta* **69**(5), 1099–1110.

Luz B. and Barkan E. (2010) Variations in $^{17}O/^{16}O$ and $^{18}O/^{16}O$ in meteoric waters. *Geochem. Cosmochim. Acta* **74**, 6267–6286.

Luz B., Barkan E., Bender M. L., Thiemens M. H. and Boering K. A. (1999) Triple-isotope composition of atmospheric oxygen as a tracer of biosphere productivity. *Science* **400**, 547–550.

Lyons J. R. (2001) Transfer of mass-independent fractionation in ozone to other oxygen-containing radicals in the atmosphere. *Geophys. Res. Lett.* **28**(17), 3231–3234.

Mahon K. I. (1996) The "new" York regression: application of an improved statistical method to geochemistry. *Int. Geol. Rev.* **38**, 293–303.

Makino A. and Mae T. (1999) Photosynthesis and plant growth at elevated levels of CO_2. *Plant Cell Physiol.* **40**, 999–1006.

Martin S., Cohu S., Vignot C., Zimmerman G. and Gattuso J.-P. (2013) One-year experiment on the physiological response of the Mediterranean crustose coralline alga, *Lithophyllum cabiochae*, to elevated pCO_2 and temperature. *Ecol. Evol.* **3**, 676–693.

Matsumi Y. and Kawasaki M. (2003) Photolysis of atmospheric ozone in the ultraviolet region. *Chem. Rev.* **103**, 4767–4781.

Mattey D., Lowry D. and Macpherson C. (1994) Oxygen isotope composition of mantle peridotite. *Earth Planet. Sci. Lett.* **128**, 231–241.

Mauersberger K., Erbacher B., Krankowsky D., Gunther J. and Nickel R. (1999) Ozone isotope enrichment: isotopomer-specific rate coefficients. *Science* **283**, 370–372.

Meijer H. A. J. and Li W. J. (1998) The use of electrolysis for accurate $\delta^{17}O$ and $\delta^{18}O$ isotope measurements in water. *Isot. Environ. Health Stud.* **34**, 349–369.

Michalski G. and Bhattacharya S. K. (2009) The role of symmetry in the mass independent isotope effect in ozone. *Proc. Natl. Acad. Sci. USA* **106**, 5493–5496.

Miller M. F. (2002) Isotopic fractionation and the quantification of ^{17}O anomalies in the oxygen three-isotope systems: An appraisal and geochemical significance. *Geochim. Cosmochim. Acta* **66**(11), 1881–1889.

Monnin E., Indermuhle A., Dallenbach A., Fluckiger J., Stauffer B., Stocker T. F., Raynaud D. and Barnola J.-M. (2001) Atmospheric CO_2 concentrations over the last glacial termination. *Science* **291**, 112–114.

Morton J., Barnes J., Schueler B. and Mauersberger K. (1990) Laboratory studies of heavy ozone. *J. Geophys. Res.* **95**, 901–907.

Muehlenbachs K. and Clayton R. N. (1976) Oxygen isotope composition of the oceanic crust and its bearing on seawater. *J. Geophys. Res.* **81**, 4365–4369.

Nagel O. W., Waldron S. and Jones H. G. (2001) An off-line implementation of the stable isotope technique for measurements of alternative respiratory pathway activities. *Plant Physiol.* **127**, 1279–1286.

Pack A. and Herwartz D. (2014) The triple oxygen isotope composition of the Earth mantle and understanding $\Delta^{17}O$ variations in terrestrial rocks and minerals. *Earth Planet. Sci. Lett.* **390**, 138–145.

Pack A., Toulouse C. and Przybilla R. (2007) Determination of oxygen triple isotope ratios of silicates without cryogenic separation of NF_3 – technique with application to analyses of technical O_2 gas and meteorite classification. *Rapid Commun. Mass Spectrom.* **21**, 3721–3728.

Rumble D., Miller M. F., Franchi I. A. and Greenwood R. C. (2007) Oxygen three-isotope fractionation lines in terrestrial silicate minerals: an inter-laboratory comparison of hydrothermal quartz and ecologitic garnet. *Geochem. Cosmochim. Acta* **71**, 3592–3600.

Sander S. P., Golden D. M., Kurylo M. J., Moortgat G. K., Wine P. H., Ravishankara A. R., Kolb C. E., Molina M. J., Finlayson-Pitts B. J., Huie R. E. and Orkin V. L. (2006). Chemical Kinetics and Photochemical Data for Use in Atmospheric Studies Evaluation Number 15. JPL Publication 06–2. Pasadena, CA, Jet Propulsion Laboratory, California Institute of Technology.

Sansjofre P., Ader M., Trindale R. I. F., Elie M., Lyons J., Cartigny P. and Nogueira A. C. R. (2011) A carbon isotope challenge to the snowball Earth. *Nature* **478**, 93–96.

Schoenemann S. W., Schauer A. J. and Steig E. J. (2012) Measurement of SLAP2 and GISP $\delta^{17}O$ and proposed VSMOW-SLAB normalization for $\delta^{17}O$ and ^{17}O excess. *Rapid Commun. Mass Spectrom.* **27**, 582–590.

Smith H. J., Wahlen M. and Mastrioianni D. (1997) The CO_2 concentration of air trapped in GISP2 ice from the Last Glacial Maximum–Holocene transition. *Geophys. Res. Lett.* **24**(1), 1–4.

Solomon S., Qin D., Manning M., Marquis M., Averyt K., Tignor M. M. B., Miller, Jr., H. L. and Chen Z. (2007) *Climate Change 2007, the Physical Science Basis*. Cambridge University Press, Cambridge.

Tanaka R. and Nakamura E. (2012) Determination of ^{17}O-excess of terrestrial silicate/oxide minerals with respect to Vienna Standard Mean Ocean Water (VSMOW). *Rapid Commun. Mass Spectrom.* **27**, 285–297.

Urey H. C. and Grieff L. J. (1935) Isotopic exchange equilibria. *J. Am. Chem. Soc.* **57**, 321–327.

Welp L. R., Keeling R. F., Meijer H. A. J., Bollenbacher A. F., Piper S. C., Yoshimura K., Francey R. J., Allison C. E. and Wahlen M. (2011) Interannual variability in the oxygen isotopes of atmospheric CO_2 driven by El Nino. *Nature* **477**, 579–582.

Wiegel A. A., Cole A. S., Hoag K. J., Atlas E. L., Schauffler S. M. and Boering K. A. (2013) Unexpected variations in the triple oxygen isotope composition of stratospheric carbon dioxide. *Proc. Natl. Acad. Sci. USA*. http://dx.doi.org/10.1073/pnas.1213082110.

Yakir D. (2003) The stable isotopic composition of atmospheric CO_2. In *Treatise on Geochemistry*, vol. 4 (ed. R. F. Keeling). Elsevier, pp. 175–212.

Yeung L. Y., Affek H. P., Hoag K. J., Guo W., Wiegel A. A., Atlas E. L., Schauffler S. M., Okumura M., Boering K. A. and Eiler J. M. (2009) Large and unexpected enrichment in stratospheric $^{16}O^{13}C^{18}O$ and its meridional variation. *Proc. Natl. Acad. Sci. USA* **106**(28), 11496–11501.

Yeung L. Y., Berelson W. M., Young E. D., Prokopenko M. G., Rollins N., Coles V. J., Montoya J. P., Carpenter E. J., Steinberg D. K., Foster R. A., Capone D. G. and Yager P. L. (2012a) Impact of diatom-diazotroph associations on carbon export in the Amazon River plume. *Geophys. Res. Lett.* **39**(L18609). http://dx.doi.org/10.1029/2012GL053356.

Yeung L. Y., Young E. D. and Schauble E. A. (2012b) Measurements of $^{18}O^{18}O$ and $^{17}O^{18}O$ in the atmosphere and the role of isotope-exchange reactions. *J. Geophys. Res.* **117**(D18306). http://dx.doi.org/10.1029/2012JD017992.

Young E. D. (2001) Reply to comment on 'Assessing the implications of K isotope cosmochemistry for evaporation in the preplanetary solar nebula' by E. Young. *Earth Planet. Sci. Lett.* **192**(1), 101–107.

Young E. D., Coutts D. W. and Kapitan D. (1998a) UV laser ablation and irm-GCMS microanalysis of $^{18}O/^{16}O$ and $^{17}O/^{16}O$ with application to a calcium–aluminium-rich inclusion from the Allende meteorite. *Geochim. Cosmochim. Acta* **62**(18), 3161–3168.

Young E. D., Galy A. and Nagahara H. (2002) Kinetic and equilibrium mass-dependent isotope fractionation laws in nature and their geochemical and cosmochemical significance. *Geochim. Cosmochim. Acta* **66**(6), 1095–1104.

Young E. D., Nagahara H., Mysen B. O. and Audet D. M. (1998b) Non-Rayleigh oxygen isotope fractionation by mineral evaporation: theory and experiments in the system SiO_2. *Geochim. Cosmochim. Acta* **62**(18), 3109–3116.

Yung Y. L., De Mone W. B. and Pinto J. P. (1991) Isotopic exchange between carbon dioxide and ozone via $O(^1D)$ in the stratosphere. *Geophys. Res. Lett.* **18**, 13–16.

Associate editor: James Farquhar